INVESTIGATION OF $N^{13,14,15}$ BOUND AND UNBOUND STATES

WITH THE ONE-NUCLEON TRANSFER REACTIONS

$C^{12,13,14}(d,n)N^{13,14,15}$

INAUGURAL DISSERTATION
FOR THE DOCTORATE DEGREE Ph.D.

OF

THE PHYSICS DEPARTMENT OF THE FREE UNIVERSITY BERLIN

INAUGURAL - DISSERTATION
ZU ERLANGUNG DER DOKTORWÜRDE

DES

FACHBEREICHS PHYSIK DER FREIEN UNIVERSITÄT BERLIN

BY

NSE MICHAEL EKPO
IKOT ESSEN AKPANTUEN
N I G E R I A

JULY 1974

Digitized by the Internet Archive
in 2026

https://archive.org/details/IA41547615_0003

INVESTIGATION OF $N^{13,14,15}$ BOUND AND UNBOUND STATES

WITH THE ONE-NUCLEON TRANSFER REACTIONS

$C^{12,13,14}(d,n)N^{13,14,15}$

INAUGURAL DISSERTATION
FOR THE DOCTORATE DEGREE Ph.D.

OF

THE PHYSICS DEPARTMENT OF THE FREE UNIVERSITY BERLIN

INAUGURAL - DISSERTATION
ZU ERLANGUNG DER DOKTORWÜRDE

DES

FACHBEREICHS PHYSIK DER FREIEN UNIVERSITÄT BERLIN

BY

NSE MICHAEL EKPO
IKOT ESSEN AKPANTUEN
N I G E R I A

JULY 1974

UNIV.
LEIDEN
BIBL.

Major Department : Physics

Chairman : Prof. Dr. J. Hoeft

1. Referee : Prof. Dr. K. H. Lindenberger

2. Referee : Prof. Dr. S. Wilking

Prom. 3. OKT. 1974

ABSTRACT

The bound and unbound nuclear states of the nitrogen isotopes $N^{13,14,15}$ have been investigated in this work with 6.3 and 6.5 MeV pulsed deuteron through one-nucleon-transfer $C^{12,13,14}(d,n)N^{13,14,15}$ stripping reactions and the resonance structure of the $C^{12,13,14}$ + p systems studied. To this end the angular distributions of the $C^{12,13,14}$(d,n)N13,14,15 reaction cross-sections were measured between zero and 82.5 degrees laboratory angle, at 13 to 17.5m neutron flight path from the target using high resolution neutron time-of-flight equipment and the 7 MV Van de Graaff accelerator in Hahn-Meitner Institute.

The obtained neutron spectra and angular distributions revealed neutron groups arising from transitions to nineteen final states in N^{14} and twenty one states in N^{15} including a new state at 11.44 MeV excitation energy (in addition to those obscured by C^{12} and O^{16} contamination in both reactions), thus enabling for the first time, states in N^{15} apart from the lowest four to be investigated through proton transfer on C^{14}. They also showed the searched-for resonance structure prominent at 2.366 MeV excitation energy in N^{13} and at 8.061 MeV in N^{14}.

The angular distributions were analysed with the help of the Distorted-Wave Born Approximation (DWBA) and Hauser-Feshbach (HF) calculations with consequent spin and parity identification of the investigated states and extraction of corresponding spectroscopic factors. This proved a test for the validity of DWBA and HF theories in describing direct interactions (DI) and compound nucleus (CN) reactions, and checked the extent to which the nucleus is described by the shell model wave functions in simple jj-coupling or with configuration mixing. Also for the first time, spectroscopic factors for states above 8.907 MeV excitation energy in N^{14} were obtained and theoretical spin-parity assignments for these states confirmed through proton transfer on C^{13}.

The s-resonsnce structure in N^{13} resulting from the (d,n) reaction was fitted with the corresponding (p,p) elastic scattering cross-section which proved that Lipperheides theory stating

that in the (d,p) reaction, the proton spectrum is given by the total off-energy shell neutron cross-section, is also valid for the relation between the (d,n) and (p,p), and actually, the unbound states neutron spectrum and cross-section are qualitatively given by the total off-energy shell proton cross-section of the (p,p) scattering. The (d,n) to (p,p) cross-section ratio revealed a dependence on the transferred resonance angular momentum.

The results of the investigation led to many new findings as regards spin, parity, spectroscopic information and resonance structure of the states in $N^{13,14,15}$ as detailed out in the summary and conclusions of chapter 7.

C O N T E N T S

CHAPTER		PAGE
	ABSTRACT	iii
1	INTRODUCTION	1
2	NUCLEAR REACTION MECHANISMS	5
2.1	Direct Interactions and Distorted-Wave Born Approximation, DWBA Theory	6
2.2	Compound Nucleus Reactions and the Hauser-Feshbach Theory	11
3	EXPERIMENTAL PROCEDURE	14
3.1	The Targets	14
3.2	The Accelerator	17
3.2.1	Beam Extraction and Acceleration	18
3.2.2	Beam Transport and Compression	19
3.3	The Detectors	21
3.3.1	Neutron Detection Process	21
3.4	Electronics	22
3.4.1	The Time Circuit	24
3.4.2	The Pulse Shape Discrimination and Energy Circuit	24
3.4.3	The Interface and the On-line-Computer	25
3.4.4	Experimental Conditions	25
4	EXPERIMENTAL RESULTS AND DEDUCTION OF DATA	27
4.1	Experimental Results	27
4.2	Deduction of Data	30
4.2.1	Neutron Energy Calibration and Spectra Identification	30
4.2.2	Extraction of Experimental Differential Cross-section	32
5	ANALYSIS OF EXPERIMENTAL DATA	37
5.1	The Optical-Potential Parameters	37
5.2	Unbound States Analysis	43

CHAPTER		PAGE
5.3	Angular Distribution Fit with DWBA and H-F Calculations	45
6	DISCUSSION	57
6.1	New Spin and Parity Information	57
6.1.1	The $C^{13}(d,n)N^{14}$ Reaction	57
6.1.2	The $C^{14}(d,n)N^{15}$ Reaction	58
6.2	The Spectroscopic Factors	60
6.2.1	Comparison of Spectroscopic Factors with Previous Measurements and Theory	62
6.2.2	S-factor Discrepancy and the Isospin Problem	69
6.3	(d,n) Stripping to Unbound States and (p,p) Elastic Scattering	71
6.4	The (d,n) to (p,p) Cross-section Ratio	74
7	SUMMARY AND CONCLUSIONS	76
	REFERENCES	79
	ACKNOWLEDGEMENTS	83
	AUTOBIOGRAPHY	84

CHAPTER 1

INTRODUCTION

The work to be presented is concerned with the investigation of bound and unbound states in the nitrogen isotopes $N^{13,14,15}$ by means of one - nucleon - transfer $C^{12,13,14}(d,n)\ N^{13,14,15}$ stripping reactions, in particular a study of the resonance structure of the $C^{12,13,14}$ + p systems in the (d,n) reaction in comparison with (p,p) elastic scattering.

The bound states of N^{14} have been the subject of many investigations in both (d,n) and (He^3,d) proton transfer on C^{13}. The present work was undertaken with special interest in the unbound states which have not at all been investigated above E_x = 8.907 MeV exitation energy, and with the aim to complement and ascertain the existing experimental information.

In the conventional pure shell model (Wa.60, Ta.60, Tr.63) the low lying T = 0, 1 states in N^{14}, assuming a C^{12} inert core with $(1s_{1/2})^4(1p_{3/2})^8$ configuration, are expected to result from three groups consisting of levels arising from 1) two particles in the ground state $(p_{1/2})^2$ configuration, 2) the mixed $p_{1/2}\ s_{1/2}$, $p_{1/2}\ d_{5/2}$ and $p_{1/2}\ d_{3/2}$ configurations and 3) the promotion of two p-shell nucleons into the degenerate or nearly degenerate sd levels resulting in $(2s_{1/2})^2$ and $(1d_{5/2})^2$ configurations. Since the C^{12} does not really form an inert core it is expected that some of the lower levels will result from $1p_{3/2}$ particles being excited out of the C^{12} core into higher orbitals giving a fourth group of levels which are known as core-exited states, like the E_x = 6.198 MeV level. To test these predictions for the higher excited, in particular the unbound states with proton transfer on C^{13} is one of the aims of the $C^{13}(d,n)N^{14}$ investigation in this work which has been done at a bombarding deuteron energy of E_d = 6.5 MeV .

The states in N^{15} have not at all been investigated through proton transfer on C^{14} except the lowest four states studied in (d,n) and (He^3,d) reactions, respectively, by Lawergren and Alford et al. (La67, Al69). There are good experimental and theoretical reasons for paying special attention to the A = 15 nuclei . In particular N^{15} has a lot of unidentified or ambigiously identified levels with regard to spin and parity (Aj70).

In pure jj-coupling (Ha57) the lowest states with positive parity (π=+) in A=15 nuclei are expected to arise from the coupling of a $2s_{1/2}$ or $1d_{5/2}$ nucleon to the A = 14 system whose ground state has $(1p_{1/2})^2_{J^\pi=0^+,1^+}$ where $J^\pi = 0^+$ for the system C^{14} and $J^\pi = 1^+$ for the N^{14} system. In the particle-hole (p-h) weak-coupling model (Li71), based on particles in the sd shell and holes in the p-shell, the negative-parity states in N^{15} are expected to be mixtures of 0p-1h, 1p-2h with T_h=0 and 1p-2h with T_h=1 configurations.

The use of C^{14} as target in reaching N^{15} is advantageous since the reduced widths from the C^{14}(d,n)N^{15} cross-sections are expected to be particulary instructive because C^{14} has zero spin and a simple wave function. The zero spin of the target should reduce ambigiuties in the J^π determination since for reactions to a definite N^{15} state, the lj-values of the transferred nucleon are fixed. Moreover the interpretation of results with a C^{14} target in terms of wave functions with lj specified for the inequivalent nucleon should be much more clear-cut than with other targets like the N^{14}(d,p)N^{15} reaction since the wave function is rather well known (Sh55) and can be more accurately determined even by the C^{14}(d,n)N^{15} experiment itself (Fr56). To identify uniquely the unknown or ambiguous spin-parity of the states in N^{15} and confirm the known spin-parity assignments in test of the shell model predictions, the C^{14}(d,n)N^{15} reaction is investigated in this work at a bombarding deuteron energy of E_d = 6.5 MeV with the ultimate aim of extracting for the first time spectroscopic information through proton transfer on C^{14} which has not existed except for the four lowest states.

The $C^{12}(d,n)N^{13}$ reaction was incorporated in this work to enhance the study of the unbound states or resonance structure in the $C^{12,13,14}$+ p systems. Apart from the spectroscopy of N^{15}, this was the main objective of the present investigation. The point of interest here is to test whether Lipperheide's theory (Li70) is valid for (d,n) stripping with respect to (p,p) elastic scattering in the same sense as has been confirmed by Fuchs et al. (Fu72) for the (d,p)-reaction versus (n,n) elastic scattering, namely that the proton spectrum in the (d,p)-stripping is given by the total off-energy shell neutron cross-section, and like the latter, occasionally shows interference between resonance and continuum scattering. Another important and verified statement of the theory is, that the ratio of the formation cross-section of a resonance as final state in stripping to that in nucleon scattering depends strongly on the l-value of the captured nucleon. Thus from a comparison of stripping and nucleon scattering a sensitive determination of l is possible.

The experiments in this work were performed with a pulsed deuteron beam at the 7 MeV Van de Graaff Accelerator in Hahn-Meitner-Institute Berlin in conjunction with high-resolution neutron time-of-flight equipment.

In chapter 2, a background is given on nuclear reaction mechanisms. The Distorted-Wave Born Approximation (DWBA) and Hauser-Feshbach methods for the analysis of experimental results from direct and compound nucleus reactions are explained in simple language. Chapter 3 deals with experimental procedures including targets, accelerator, beam extraction and transport, detectors, electronics and on-line computer data processing. Chapter 4 gives the experimental results from all three reactions and explains the method of data deduction and experimental cross-section extraction. In chapter 5, the experimental results are analysed using the DWBA and Hauser-Feshbach calculations with the optical-potential forms and best-fit parameters given. A method of unbound-states analysis which at the moment was not within reach of direct DWBA and H-F calculations is presented. The experimental and theoretical angular distributions for $C^{13,14}(d,n)N^{14,15}$ reactions are also presented with the fits discussed, the J^{π}-values determined (or limited)

and spectroscopic information extracted. Chapter 6 discusses the spin-parity and spectroscopic-information results, compares the spectroscopic factors with previous measurements and theory, with special interest in the transition strengths of the mirror states in the N^{15} and O^{15} mirror nuclei, and further discusses the strength discrepancies including isospin anomaly between the (d,n) and the (He^3,d) reaction for the T = 1 lowest state in N^{14}. The (d,n) and (p,p) resonance structure studies are presented with an informative example from the $C^{12}(d,n)N^{13}$ reaction . The results of the (d,n) to (p,p) cross-section ratio studies are also presented in chapter 6. Chapter 7 gives a summary and conclusions of the whole investigation.

CHAPTER 2

NUCLEAR REACTION MECHANISMS

To analyse the angular distributions of the experimental cross-sections for the extraction of spectroscopic information demands a knowledge of the reaction mechanism and the theories behind it.

Nuclear reactions are in general classified into direct interactions (DI) and compound nucleus (CN) reactions, with the main difference in the time taken by the process in each case. The reaction time for DI is of the order of 10^{-22} sec, and for CN, about 10^{-16} - 10^{-20} sec (the time domain of 10^{-20} sec is attributed to intermediate reactions (IR) leading to doorway states).

The incident particle entering the nucleus experiences for the most part, an average potential and, on occasion makes a close collision with a target nucleon in which the target nucleus is excited. At high energy, this collision gives rise either to a direct reaction or results in a doorway state if the energy loss is large and the particle is trapped into a bound state. Also it becomes possible for the incident particle to have several further collisions thus giving rise to complicated compound nucleus (CN) states. The same way back into the elastic channel is always possible.

The maximum factor of 10^{6} time delay for CN reaction compared to the direct reaction is caused by the fact that many collisions are required for a particle to regain the energy necessary for escape out of the nucleus. The long live time of the CN states gives rise to a strong energy dependence in the cross-sections. A direct consequence of the short interaction time of the DI is that the cross-sections for this mechanism exhibit slow variations with incident energy. Angular distributions for DI are characterized by strong forward and/or back angle peaking while that of CN is symmetric about 90^{o} or almost isotropic.

Though nuclear reactions are classified into two extremes, DI and CN, both mechanisms are important and the proper description of any reaction must include both as they interfere with each other (Er62) and their transition amplitudes contribute to form the reaction cross-section

$$\begin{aligned} \sigma &= \text{const.}|T_{DI} + T_{CN}|^2 \\ &= \text{const.}\{|T_{DI}|^2 + |T_{CN}|^2 + 2\text{Re } T_{DI}T_{CN}^*\} \\ &= \sigma_{DI} + \sigma_{CN} + \text{const. } 2\text{Re } T_{DI}T_{CN}^* \end{aligned} \qquad 2.1$$

where T_{DI}, T_{CN} - transition amplitudes of DI and CN reactions,

$\text{const.}T_{DI}T_{CN}^*$ - interference term of the DI and CN.

The two terms comprising of T_{CN} fluctuate strongly as a function of energy. But while $|T_{CN}|^2$ has only positive contributions, $\text{Re } T_{DI}T_{CN}^*$ takes positive and negative values. Its energy average is zero, therefore, if the cross-section to be analysed is an energy average, either by calculation, by poor energy resolution, or through overlap of many compound levels, it is correctly described by the incoherent sum $\sigma_{DI} + \sigma_{CN}$.

The direct interaction mechanism is accounted for by the Distorted Wave Born Approximation theory (To61), while the compound-nucleus reaction in case of many overlapping compound states is treated by the Hauser-Feshbach statistical theory (Ha52).

2.1 Direct Interactions and Distorted Wave Born Approximation (DWBA) Theory

The DWBA used in calculating the transition amplitudes T_{DI} in Eg.2.1 has received wide treatment in various works (To61, Au62, Ba62, Hu65, Sa64,65).

The direct interaction theory and DWBA assume that :

1) The incoming particle or nucleus interacts with only one or few of the nucleons in the target nucleus.

2) The one or two internal degrees of freedom of the system involved in the interaction are describable in terms of single-particle mode of motion.
3) The interaction peaks on the nuclear surface.
4) The elastic scattering is the most important process which occurs, while inelastic events are treated as perturbations.

Consequently the DWBA expression for the transition amplitude describe a single-step process. The relative motion before and after the inelastic event is described by distorted-waves which describe the elastic scattering.

DWBA has the advantage of taking into account the influence of the nuclear interior (strong absorptions) through appropriate distorted waves, namely the use of an imaginary potential. Distortion effects in DWBA modify the differential cross-section and the angular distribution. More-over DWBA theory predicts absolute cross-sections necessary to extract nuclear-structure factors which is the main purpose of this work. On the other hand DWBA calculations depend on parameter juggling which disquises the advantages of the method.

In the reaction of type A(d,n)B , the incident deuteron with internal wave function $\psi_d(|\vec{r}_{nA} - \vec{r}_{pA}|)$, kinetic energy T_{dA} and internal energy T_{np}, sees in the vicinity of the target nucleus A having a wave function $\psi_A(\xi)$ and energy H_A, an optical potential $\bar{V}_{dA}$ of the target nucleus which distorts the deuteron wave function into a wave $\phi_i^{(+)}(\vec{k}_d, \vec{r}_{dA})$. The deuteron components (proton and neutron) experience the potential V_{pA}, V_{nA} respectively and, disrupted of the neutron-proton binding potential V_{np}, the deuteron is stripped of its proton which is captured by the potential V_{pA} of the target nucleus to form a residual nucleus B in the ground or excited state with wave function $\psi_B(\xi, \vec{r}_{pA})$ and internal energy $H_A + T_{pA}$, while the neutron flies away with kinetic energy T_{nB} under the influence of an optical potential $\bar{V}_{nB}$ giving the wave function $\phi_f^{(+)}(\vec{k}_n, \vec{r}_{nB})$.

In formal reaction and scattering theory, the depicted process is described by the following exact expression for the reaction

amplitude (in the post formulation)

$$T = \left\langle \phi_f^{(-)}(\vec{k}_n, \vec{r}_{nB}) \psi_B(\xi, \vec{r}_{pA}) \middle| V_{np} + V_{nA} - \bar{V}_{nB} \middle| \Psi_i^{(+)} \right\rangle \qquad 2.2$$

where

$\phi_f^{(-)}(\vec{k}_n, \vec{r}_{nB})$ - the optical-model wave function of a neutron going out with momentum $\vec{k}_n$, calculated with the optical potential $\bar{V}_{nB}$,

$\Psi_i^{(+)}$ - the exact wave function of the total Hamiltonian of the system with the boundary condition of an incoming deuteron wave of momentum $\vec{k}_d$.

The initial total wave of the system includes all reaction channels in the form

$$\Psi_i^{(+)} = \Psi^+(d,d)_{elastic} + \Psi^+(d,d')_{inel.} + \Psi^+(d,n)_{reaction} + \text{others} \qquad 2.3$$

According to reaction theory, the operators in the matrix element are those potentials of the total Hamiltonian which are neglected in calculating the approximative outgoing-wave function $\phi_f^{(-)}\psi_B$ on the right hand side of Eg.2.2, namely the difference between the exact interaction (consisting of A and p) and the approximate optical model interaction.

In order to arrive at expressions allowing practical calculations, the exact expression 2.2 must be modified by several approximations (DWBA approximations) :

1) The exact wave function $\Psi_i^{(+)}$ in 2.2 is replaced by the corresponding distorted wave (neglecting other channels in 2.3 except the elastic channel)

$$\Psi_i^{(+)} \rightarrow \psi_d(|\vec{r}_{nA} - \vec{r}_{pA}|)\phi_i^{(+)}(\vec{k}_d, \vec{r}_{dA})\psi_A(\vec{\xi}) \qquad 2.4$$

This means that the transition amplitude is calculated in first order perturbation.

2) The difference $(V_{nA}-\bar{V}_{nB})$ is neglected, which means that the exact interaction between the neutron and the target nucleus A is replaced by the optical potential in the exit channel.

3) Assuming a zero-range approximation as calculational convenience of reducing six-dimensional integration in the $\vec{r}_d$, $\vec{r}_{nB}$-space to three, by making $\vec{r}_d$ parallel to $\vec{r}_{nB}$ on assumption that the neutron is emitted at the same point at which the deuteron is absorbed so that $\vec{r}_n=(A/B)\vec{r}_d$ where A, B are the masses of the target and residual nuclei. The zero-range approximation is made by setting

$$\psi_d(|\vec{r}_{nA} - \vec{r}_{pA}|)V_{np}(|\vec{r}_{nA} - \vec{r}_{pA}|) = D_o\delta(|\vec{r}_{nA} - \vec{r}_{pA}|) \qquad 2.5$$

The evaluation of the transition amplitude is performed by making partial-wave expansions of the distorted waves obeying angular momentum coupling rules including spin-orbit coupling.

An important feature of the single-nucleon transfer is that the overlap of the participating nuclear states factorizes out of the T - Matrix in the form

$$\left\langle \psi_B^* | \psi_A \otimes \phi_{\ell j} \right\rangle = S_{\ell j}^{1/2} \qquad 2.6$$

or writing angular momentum quantum numbers explicitly,

$$\left\langle \psi_{JB}^*(\xi, \vec{r}_{pA}) | \psi_{JA}(\xi) \otimes \phi_{\ell j}(\vec{r}_{pA}) \right\rangle = S_{\ell j}^{1/2} \qquad 2.7$$

where the symbol $\otimes$ denotes angular-momentum coupling, and $\phi_{\ell j}(\vec{r}_{pA})$ is a single-particle wave function for the built-in proton calculated with a one-body shell model potential $V(\vec{r}_{pA})$.

The squared nuclear overlap $S_{\ell j}$ is called the "spectroscopic factor", and contains the desired spectroscopic information. It gives the probability of finding in the residual state, the target ground state with a proton in the orbit ℓj coupled to it to give the final spin J_B .

After series of operations, one arrives at the following final expression for the cross-section (Sa64)

$$\frac{d\sigma}{d\Omega}(\theta) = 1.48 \frac{2J_B+1}{2J_A+1} C^2 S_{\ell j} \sigma_{\ell j}^{DWBA}(\theta) = M_{DW} \sigma_{\ell j}^{DWBA}(\theta) \qquad 2.8$$

The overall normalization factor 1.48 is essentially determined by the strength D_o of the neutron-proton interaction (Eq.2.5). The Clebsch-Gordan coefficient C takes care of the isospin coupling of the transferred proton and the target to give the isospin of the final state. The cross-section is directly proportional to the spectroscopic factor $S_{\ell j}$, the square of the nuclear overlap (Eqs. 2.6 and 2.7)

The cross-section $\sigma_{\ell j}^{DWBA}(\theta)$ for a transition with uniquely defined ℓ and j transfer is the quantity calculated by current DWBA codes and is given as

$$\sigma_{\ell j}^{DWBA}(\theta) = \frac{\mu_n \mu_d}{(2\pi\hbar^2)^2} \frac{k_n}{k_d} \sum_{m M_n M_d} |\beta_j^{\ell m M_n M_d}(\theta)|^2 \qquad 2.9$$

where

$$\beta_j^{\ell m M_n M_d}(\theta) = \sum_{L_d L_n J_d J_n} \Gamma_{L_n J_n L_d J_d}^{\ell j m M_n M_d} P_{L_n}^{M_n}(\theta) f_{L_n J_n L_d J_d}^{\ell j} \qquad 2.10$$

Thus after seperating the nuclear structure part contained in $S_{\ell j}$, the kinematic aspect of the transfer is described by the cross-section $\sigma_{\ell j}^{DWBA}(\theta)$ of the outgoing neutron, which quite naturally is given as an expansion in Legendre polynomials $P_{L_n}^{M_n}(\theta)$ for neutrons going at the angle θ. The weight of each Legendre polynomial $P_{L_n}^{M_n}(\theta)$ is given by two factors, each of which has a simple and intuitively understandable significance. The first is the magnitude Γ, simply consisting of angular momentum coupling coefficients describing the probability that the partial wave L_n, J_n, M_n of the outgoing neutron and the momenta ℓ, j, m of the built-in proton may be combined to a given partial wave L_d, J_d, M_d of the impingent deutron. The second factor is the "radial integral",

$$f_{L_n J_n L_d J_d}^{\ell j} = \frac{2\pi^{1/2}}{k_n k_d} \frac{M_B}{M_A} \int_o^\infty dr \, \phi_{L_n J_n}(k_n, \frac{M_A}{M_B} r) \, \phi_{\ell j}(r) \phi_{L_d J_d}(k_d, r) \qquad 2.11$$

which is the radial overlap of the combined partial waves. The functions Φ_{LJ} are the radial wave functions of the corresponding partial waves, and $\phi_{\ell j}(r)$ is the radial part of the bound wave function of the transfered proton.

2.2 Compond Nucleus Reactions and the Hauser-Feshbach Theory

The CN reaction amplitude and cross-section in 2.1 is usually determined through the use of Hauser-Feshbach (Ha52) formalism with inherent assumptions that:

1) The CN decay is independent of its mode of formation.

2) The decay depends only upon its energy, angular momentum and parity.

3) All possible decay products are treated in a democratic fashion based on liquid drop evaporation model.

4) Time reversal invariance holds.

That the CN decay loses all memory of how it was formed (1) permits the CN cross-section to be decomposed into the probability for CN formation σ_α through channel α with

$$\sigma_\alpha = \frac{\pi}{k_\alpha^2} T_\alpha \qquad 2.12$$

and the probability for CN decay P_β through a particular exit channel β where

$$P_\beta = \frac{T_\beta}{\sum_\gamma T_\gamma} , \qquad 2.13$$

T_α, T_β, T_γ - Transmission coefficients in the entrance channel α and exit channel in question β, and all possible outgoing channels γ ($\sum_\gamma P_\gamma = 1$).

α, β, γ - characterize the entire quantum description of the respective channels such as angular momentum and parity involved.

The net cross-section for the CN reaction is

$$\sigma_{CN} = \sigma_\alpha P_\beta = \frac{\pi}{k_\alpha^2} \frac{T_\alpha T_\beta}{\sum_\gamma T_\gamma} \qquad 2.14$$

The transmission terms account for barrier penetrabilities in CN formation and decay. The differential cross-section involves Racah algebra (Bi52) to effect momentum coupling. According to the Hauser-Feshbach theory, the explicit expressions (Ha52, Bi53, Sa56, De57, Fe60, Vo68) contain Racah functions as numerical weighting factors and spherical harmonics describing the angular dependence. For the deuteron stripping, the differential cross-section has the form

$$\sigma_{CN} = M_{HF}\, \sigma^{HF}(\theta) = \frac{M_{HF}}{4k_d(2J_A+1)(2s_d+1)} \sum_{\alpha\beta} A_{\alpha\beta} \frac{T_\alpha T_\beta}{\sum_\gamma T_\gamma} \qquad 2.15$$

where M_{HF} - absolute normalization factor,

k_d - wave number of the deuteron's relative motion in the entrance channel,

s_d - spin of the deuteron,

J_A - spin of the target nucleus,

$A_{\alpha\beta}$ - Racah weighting factors and spherical harmonics (geometrical factor).

The transmission coefficients are calculated through the use of the imaginary part of the optical potential which describes the disappearance from the elastic channel of the incident particle into the channel concerned. The normalization factor M_{HF} is assumed to account for the reduction due to the loss of flux into direct reactions in each channel and takes into consideration the fluctuations of the spectroscopic factor and hence the direct reaction flux into the final states. Under the assumption of no direct-reaction contribution, M_{HF} should be the same for all

channels. The value of M_{HF} is determined usually through comparison of σ^{HF} with the experimental cross-section in the expression

$$\sigma^{exp}(\theta) = M_{DW}\, \sigma^{DWBA}_{\ell sj}(\theta) + M_{HF}\, \sigma^{HF}(\theta) \qquad 2.16$$

Here M_{HF} is treated as an adjustable parameter and comprises also the (state-independent) denominator $\sum_{\gamma} T_{\gamma}$, which is not calculated explicitly.

CHAPTER 3

EXPERIMENTAL PROCEDURE

The measurements were performed with the Van de Graaf Accelerator in the Hahn-Meitner Institute Berlin, using the time-of-flight technique. The carbon targets were bombarded with a 6.5 MeV pulsed deuteron beam from the accelerator supplying a target current of about 1μA. The outgoing neutrons were picked up by a set of twelve NE 213 liquid scintillator detectors mounted on XP 1040 photomultipliers, arranged 7.5 degrees apart between zero and 82.5 degrees lab. angle, at 13 to 17.5 m flight paths from the target.

3.1 The Targets.

The $C^{12,13}$ targets, supplied by the Nuclear Physics Sector target Laboratory, consisted of a selfsupported 9.7μg/cm^2 C^{12} target and 95μg/cm^2 C^{13} deposited by thermal cracking onto a tantalum backing. The thicknesses were determined by weighing. The C^{13} target was 98% enriched.

The 74% enriched C^{14} target, a loan from the I. Staatsinstitut für Physik der Universität Hamburg (after suffering long use) was deposited on gold backing by operating an electrical discharge in C_2H_2. Attempts to prepare the C^{14} target in our laboratory was not rewarded with fruits due to problems arising from the conversion of the only available sample of methyle Iodide into C_2H_2.

The supplied C^{14} target, claimed to have a thickness of 125μg/cm^2 showed a marked deterioration from previous use through sputtering and was consequently checked with β-decay measurement to determine the exact density.

With a half life $T_{1/2}$ = 5730 yrs, C^{14} decays by emitting β-particles of maximum energy E_β = 0.2 MeV. The emitted particles were

counted with a β-counter (Pr64) by exposing at a time an area $A = 0.2cm^2$ of the target surface to the window of the β-proportional counter. By repeated exposures accross the target surface horizontally and vertically, the distribution of C^{14} atoms in the target was obtained as shown in Fig.1 .

The sharp fluctuations in counts/sec show the inhomogeneity of the target surface. Areas with minimum counts in both directions demonstrate the sputted areas on the target surface due to previous repeated use. The source strength S was obtained from n, the average counts per sec, as

$$S = \frac{n}{G f_b f_s f_w} \qquad 3.1.1$$

where G - geometrical factor of the counter window,

f_b - target backing backscattering factor,

f_s - target self-scattering and self-absorption coefficient,

f_w - source to counter interior absorption coefficient.

The number of C^{14} atoms N in the exposed target area was obtained from the source strength through the decay equations

$$-\frac{dN}{dt} = \lambda N = S \qquad 3.1.2$$

where $\lambda = \frac{0.693}{T_{1/2}}$ - the decay constant.

The mass M of C^{14} within the exposed target area A is given by the equation

$$M(g) = 14 \frac{N}{N_L} \qquad 3.1.4$$

where $N_L = 6.024 \times 10^{23}$ - the Avogadro's number.

The target surface density or thickness is then given by

$$T = \frac{M}{A} = 14 \frac{N}{AN_L} \frac{S}{\lambda} \quad (g/cm^2) \qquad 3.1.5$$

From Eq.3.6 the absolute surface density of the C^{14} target was calculated to be T = 10.7 $\mu g/cm^2$ $\pm$ 25%, the error arising from a) target inhomogenity (10%), b) geometrical correction (5%), c) f_b, f_s, and f_w factors (7%) and d) electronic dead time correction (3%).

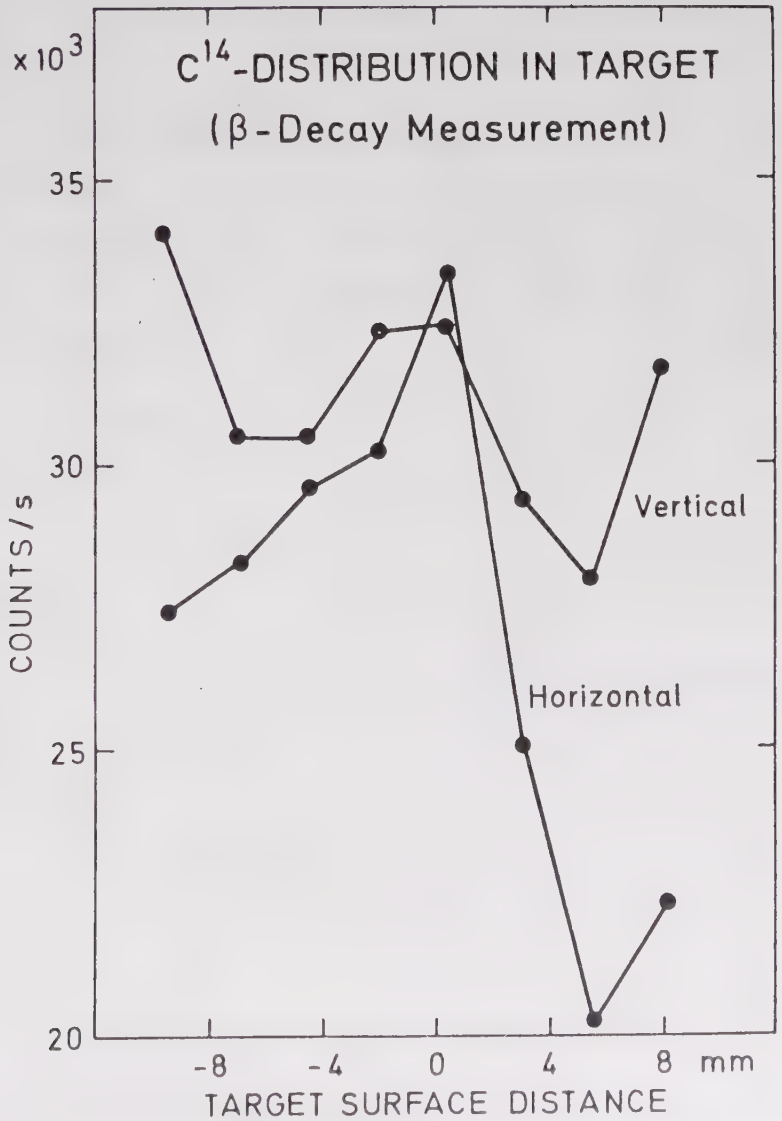

Fig.1 - Distribution of C^{14} in the Target.

3.2 The Accelerator

The 7 MV Van de Graaff accelerator in Hahn-Meitner Institute is capable of producing charged particles such as p, d, α and He^3 as well as doubly charged He^3 particles in which case a stripper is easily inserted along the accelerator tube with consequent drop in the accelerator's maximum voltage of 7 MV.

Fig.2 shows the Van de Graaff accelerator with the beam transport system for the (d,n) time-of-flight measurement.

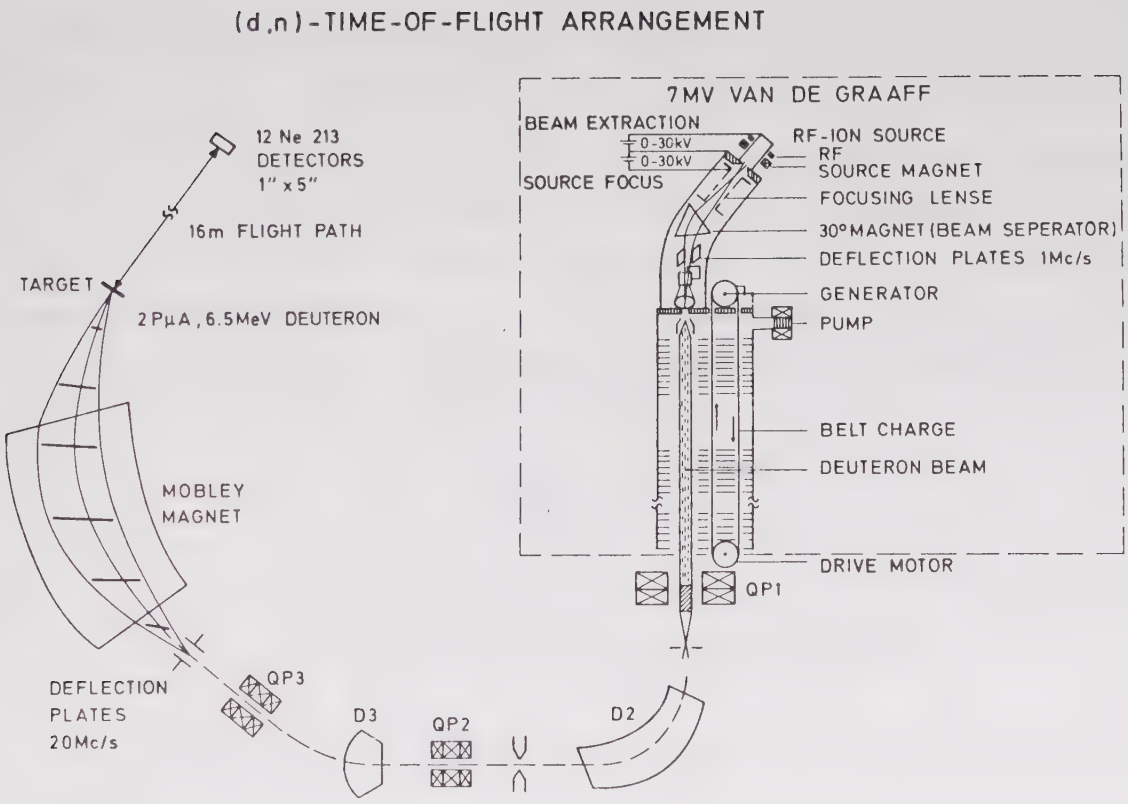

Fig.2 - A view of the 7 MV Van de Graaff accelerator with the beam transport system. QP - quadrupole lense, D2 - 90° analysing magnet, D3 - switch magnet.

3.2.1 Beam Extraction and Acceleration

At about 10^{-6} Torr ion source (10^{-4} accelerator) vacuum, deuterium gas was constantly led into the RF-ion source through a thermo-valve and the gas flow maintained at (2-25)cm^3/hr . Within the ion source, the deuterium atoms were stipped of their single orbital electrons into ions by the high radio frequency of 145 MHz, and 500 W maximum transmission. The free electrons were attracted to the beam extraction anode, while the source magnet offered a magnetic field with consequent longer way for the electrons to spiral up to the anode, thus increasing the ionization probability as electrons induced more ionization through multiple collisions with the gas molecules before reaching the anode. This process gave a continuous rise of ion avalanche interupted only by low electron-ion recombination.

The ion avalanche was drawn towards the beam extraction cathode, pre-accelerated to about 45 kV by the source focuse, and with the help of electrostatic (focusing) lenses focused onto the 30^{o} analysing magnet or beam seperator (Fig.2). Apart from deuteron particles, the focused ion beam contained various ion contaminants such as p, α^{+}, He^{3+} etc. arising from gas impurities in the ion source. The 30^{o} magnet of resolving power $m/\Delta m = 17$ extracted from the ion beam only particles of desired charge Ze, and mass m, governed by the magnetic field B and radius of curvature

$$\rho = \frac{p}{ZeB} = \frac{(2mE)^{1/2}}{ZeB} \qquad 3.2.1$$

where p - the particle's momentum,
E - the particle's kinetic energy

and focused the extracted beam through a 3mm hole below the deflection plates.

The continuous flow of the extracted d-beam through the hole was broken up into pulses of 10 nsec duration by the deflection plates ($V_{max.} = \pm 235$) which rotated the beam such that the 3mm-hole was encountered at a frequency of 1 MHz, or 1μsec, while the beam flow through it lasted 10 nsec . The pulsed d-beam was then focused

by grid lenses into the accelerator tube and then accelerated to a deuteron energy of E_d = 6.5 MeV for further transport.

3.2.2 Beam Transport and Compression

The electrodes of the accelerator tube together with a quadrupole lense QP1 and an electrostatic deflector, (Fig.2) focused the accelerated d-beam into the entrance of the 90° analysing magnet.

The 90° magnet deflected the beam to a focus in a direction perpendicular to the beam's original axis with angle of deflection corresponding to the magnet's wedge angle of 90°. The magnetic field strength B was used in measuring the particles energy and was itself measured by method of proton resonance. The particle energy was maintained constant by an amplifying regulator connecting the magnet's exit slits with the accelerator's corona. The two magnetic quadrupole lenses QP1, QP2, and the switching magnet D3 served in directing and focusing the beam into the mobley magnet for compression (Mo63).

Before entering the mobley magnet for further reduction to 1 nsec pulse duration, the beam passed the 20 MHz deflection plates. With suitable phase, the sinus shaped high-frequency alternating voltage of the deflection plates set the beam-front in a slanting position to its original direction. In the mobley magnet, the particles in the forfront underwent a longer distance than those behind such that a timely compression of the beam to 1 nsec duration was obtained at the target.

The terminal of the beam tube after the mobley magnet is shown in (Fig.3) carrying the target T, which constitutes a direct terminal of the beam-tube vacuum system. The target sits on a valve finger which facilitates the change of targets within minutes. A bellow permits a conical movement of the finger valve, such that the heat resulting from target bombardment by deuterons is distributed over the target surface. Additional cooling was afforded by compressed air. Three tantalum diaphragms or blinds

prevented contributions of (d,n) reactions on light nuclei from tube material (aluminium) which could constitute sources of high background. By the beam flow, the two brass tubes (pick-up-tubes) were influenced, one of which gave a signal for continuous control of the beam profile while the other offered a stop signal for the time-of-flight measurement.

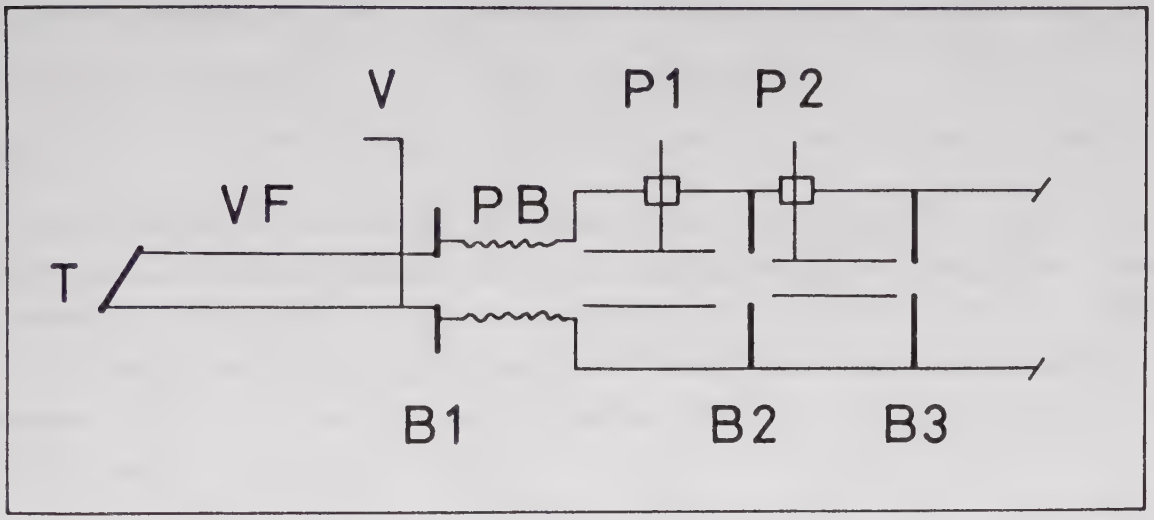

Fig.3 - Schematic diagram of the beam tube terminal. T - target, VF - valve finger, B - blinds (tantalum), PB - parallel bellow, P - pick-up-tubes, V - valve.

Table 3.1 gives the dimensions of the beam tube terminal components.

Table 3.1 - Beam tube terminal dimensions

Blinds	Diameter	Target to blind distance	
B1	3 cm	T - B1	20 cm
B2	3.5 cm	T - B2	42 cm
B3	6x2.3 (breadth x height)	T - B3	53 cm

The beam qualities at the target are given in Table 3.2 for the three reactions $C^{12,13,14}(d,n)N^{13,14,15}$.

Table 3.2 - Beam qualities at the target.

Beam energy	6.5 MeV
Beam current	1 - 1.2μA direct current.
Beam pulse duration	0.5 nsec full width at half max.
Beam pulse frequency	1 MHz or 1 μsec.

The groups of neutrons arising from the (d,n) reactions on the carbon isotopes were picked up by a set of twelve detectors arranged between 0° and 82.5° at an interval of 7.5° lab. angle. Detectors 1-8 were set at a distance of 17.5m from the target while detectors 9,10, 11 and 12 were limited by space respectively to 16, 15, 13.8 and 13 m flight paths.

3.3 The Detectors

Organic scintillator NE213 filled in a 1" x 5" aluminium capsule was used for detecting the fast neutrons. The scintillator was mounted onto a photomultiplier of type XP1040 (Valvo) carried by a pre-amplification unit (Pre-Amp), (Fig.4), through which high voltage was supplied to the photomultiplier dynodes. The ensuing pulses from the photomultiplier were pre-processed in the pre-amplification unit (Ha66).

3.3.1 Neutron Detection Process

The fast neutrons were detected through n-p elastic scattering in the liquid scintilator . The neutrons gave up their energies to the scattered protons which in their flight knocked electrons out of their sites in the scintillator atoms. In readjustment processes in which electrons fell back from upper atomic shells to

fill these vacancies, photons were emitted which were transformed into electric pulses when they struck the cathode of the photomultiplier and knocked out electrons. The number of electrons increased with the dynodes giving a total charge Q at the last dynode or anode which gave through a capacitor C an output Voltage $V_{out} = Q/C$.

The process by which electrons dropped into the vacancies in the scintillator atoms is an exponential decay whence the number of emitted photons and hence the charge Q varies as the integral of that equation in the form

$$Q(t) \propto \int_0^{\infty} \lambda_\upsilon e^{-\lambda_\upsilon t}\, dt \propto 1 - e^{-\lambda_\upsilon t} \qquad 3.3.1$$

where λ_υ - the decay constant for vacancies in the scintillator atom.

The output pulse has a rise time of $t_r \approx 2.2/\lambda_\upsilon$.
The decay constant of pulses arising from protons is different from that of pulses arising from electrons. This allows the discrimination between neutrons and γ-rays.

The size of the output pulse is proportional to the number of electrons emitted from the photocathode, which is proportional to the number of photons emitted in the scintillator, which is proportional to the number of electrons knocked out of their atomic shells, which is proportional to the energy lost by the recoil protons.

3.4 Electronics

The electronics used in the neutron energy detection is conventional with modernized components (Bu72). Adjusted to suit an on-line computer, the set of twelve detectors were divided into three groups of four detectors each and the electronic system is shown in the block diagram of Fig.4.

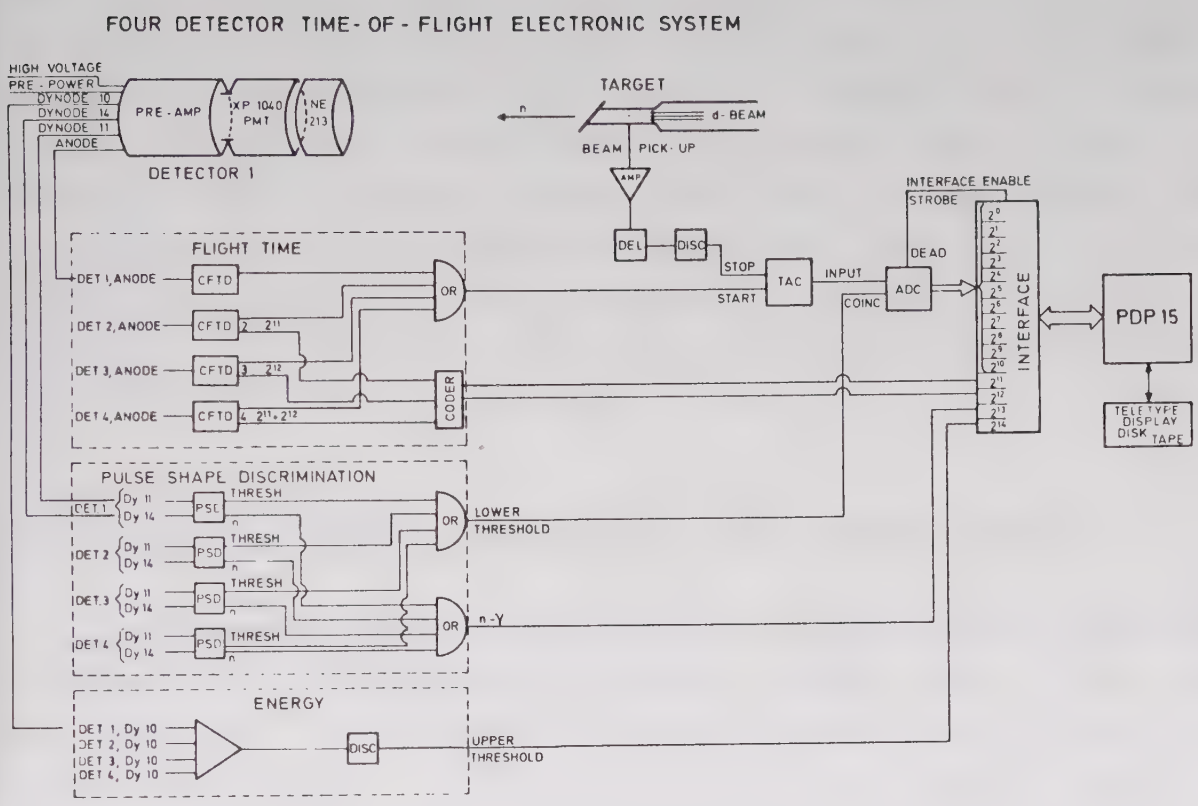

Fig.4 - Block diagram of the neutron time-of-flight electronics. PRE-AMP - pre-amplification unit; CFTD - constant fraction time discriminator; PSD - pulse shape discriminator; DISC - discriminator; OR - logical input/output unit; AMP - amplifier; TAC - time-to amplitute converter; ADC - analog-to-digital-converter.

3.4.1 The Time Circuit

The time between the target bombardment by the deuterons and the neutron detection in the detector is measured with the Time-Amplitude-Converter TAC. The time signal from each four detectors was taken from the anode of the photomultiplier with a set of Constant-Fraction-Time-Discriminator of Ortec.Type 453, and passed through an OR to start the TAC which was stoped by the delayed beam-peak-up signal. The time spectrum was digitalized in a 2048-Channel Analog-Digital-Converter (ADC) of type Laben Mod. FC60. Here only events which were in coincidence with those from the lower threshold in the pulse shape discrimination circuit were registerd and transferred to the PDP-15 computer through an interface. The coder was used to correlate the separate detector information.

3.4.2 The Pulse Shape Discrimination and Energy Circuit

The threshold energy is a standard measure of the detectors efficiency. The lower-threshold signal of each group of four detectors was taken from dynode 11 of the photomultiplier through Pulse Shape Discriminators (PSD), and united with an OR, was brought into coincidence with the time signal through an analog mixer and a discriminator.

The properties of the NE213 scintillator (Sect.3.3.1) permitted pulses arising from neutrons to be differentiated from those coming from γ-rays as background. The n/γ signal taken from dynode 14 of each photomultiplier with a pulse shape discrimination unit and brought together through an OR, was fed directly to the interface. The used method of pulse shape particle discrimination (Rö65) was able to suppress up to about 99% of the γ-bacground.

For measurements of a large range of neutron energy, an upper threshold energy setting is useful because it offers a cleaner spectrum for the high-energy neutrons. The upper threshold signal was taken from dynode 10 of each four detectors and after amplification was fed through a discriminator into the interface.

3.4.3 The Interface and the On-line-Computer

In the interface, bits were set stepwise for the ADC-word, for the separate detector signal arriving through the coder, and for the n/γ - differentiation and energy threshold, such that in the computer, events in each detector can be identified and stored according to the n/γ signal and the threshold. The events were sequentially transferred from the ADC to the computer and stored on a magnetic tape as well as in the computer memory which enabled a screen observation of the time-of-flight spectrum in 512 channels during measurement.

The stored information consisted of:

a) flight-time-information (12 bits),
b) detector information (2 bits = 4 combinations for 4 detectors),
c) a bit for pulse shape discrimination (0 = γ , 1 = n), and
d) one bit for the two thresholds.

To obtain the time-of-flight spectrum, the magnetic tapes were processed with the computer SIEMENS 4004/55(151) using a replay-procedure.

3.4.4 Experimental Conditions

The electronics was tested and the threshold energies set (NIM72) using a PuBe radio active sample (E_n^{max} = 10.250 MeV, E_γ^{max} = 4.442 MeV, and E_e^{max} = 4.191 MeV). The threshold energies and other data showing the conditions fulfilled for the three reactions during the experiment are summarized in Table 3.3.

Table 3.3 - Summary of experimental conditions.

Type of reaction	$C^{12}(d,n)N^{13}$	$C^{13}(d,n)N^{14}$	$C^{14}(d,n)N^{15}$
Target thickness	9.7μg/cm^2	95μg/cm^2	10.7μg/cm^2
Target percentage content	98%	97%	74%
Target inclination†	0°	20°	0°
Detector - target distance	17.5m	Det. 1-8, 9, 10, 11, 12. 17.5,16, 15,13.8,13m	
Angles of measurement	0°	0° - 82.5°, $\Delta\theta$ = 7.5°	
Deuteron beam energy	6.3 MeV	6.5 MeV	6.5 MeV
Beam current (average)	0.86μA	1.1μA	1.1μA
Beam pulse duration(FWHM)	0.8 nsec	0.53 nsec	0.52 nsec
Total beam charge	0.94x10^{4}μC	1.63x10^{4}μC	4x10^{4}μC
Lower threshold energy	1.8 MeV	1.8 MeV	1.8 MeV
Upper threshold energy	3.78 MeV	3.78 MeV	3.78 MeV
Measurement time	3hr	4hr	14hr

† The target inclination is the angle between the target surface and the plane perpendicular to the beam direction. The effective target thickness is given with respect to the angle of inclination θ as

$$T_{eff}(\theta) = T/\cos\theta \qquad 3.4.1$$

where T - the given or weighed target thickness.

CHAPTER 4

EXPERIMENTAL RESULTS AND DEDUCTION OF DATA

4.1 Experimental Results.

Typical time-of-flight spectra arising from the $C^{12}(d,n)N^{13}$, $C^{13}(d,n)N^{14}$, and $C^{14}(d,n)N^{15}$ reactions are shown in Figs.5-7 .

Fig.5 shows the spectrum for the $C^{12}(d,n)N^{13}$ reaction at a laboratory angle of $\theta_{Lab.} = 0^{\circ}$ with the ground state contaminated by neutrons from the $C^{13}(d,n)N^{14}$ reaction.

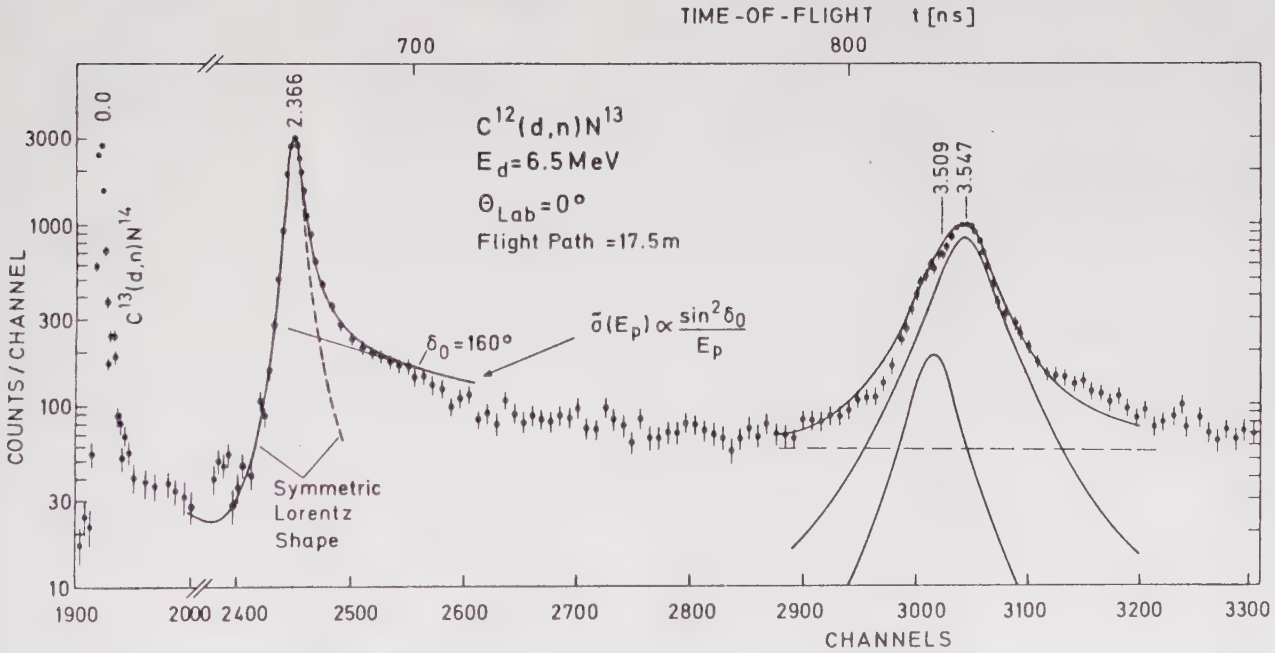

Fig.5 - Time-of-flight spectrum of neutrons from the $C^{12}(d,n)N^{13}$ reaction at deuteron energy of E_d = 6.5 Mev.

The unresolved doublet of unbound states at E_x = 3.509 MeV and E_x = 3.549 MeV excitation energies, were separated using the Lorentz shape. For this doublet, the lower solid curves represent the individual levels while the curve through the experimental points represents their sum, including the background (horizontal broken line). The error bars are statistical.

The assymmetric shape of the unbound first excited state E_x = 2.366 MeV is dicussed in detail in Sect.6.3 .

The time-of-flight spectra of neutrons from the $C^{13}(d,n)N^{14}$ reaction (Fig.6) show states with T = 0 prominent in the foward angle $\Theta_{Lab} = 0^o$. Seen also are contaminant peaks from $C^{12}(d,n)N^{13}$ and $O^{16}(d,n)F^{17}$ reactions. The region of unbound levels begins at an excitation energy of E_x = 7.55 MeV .

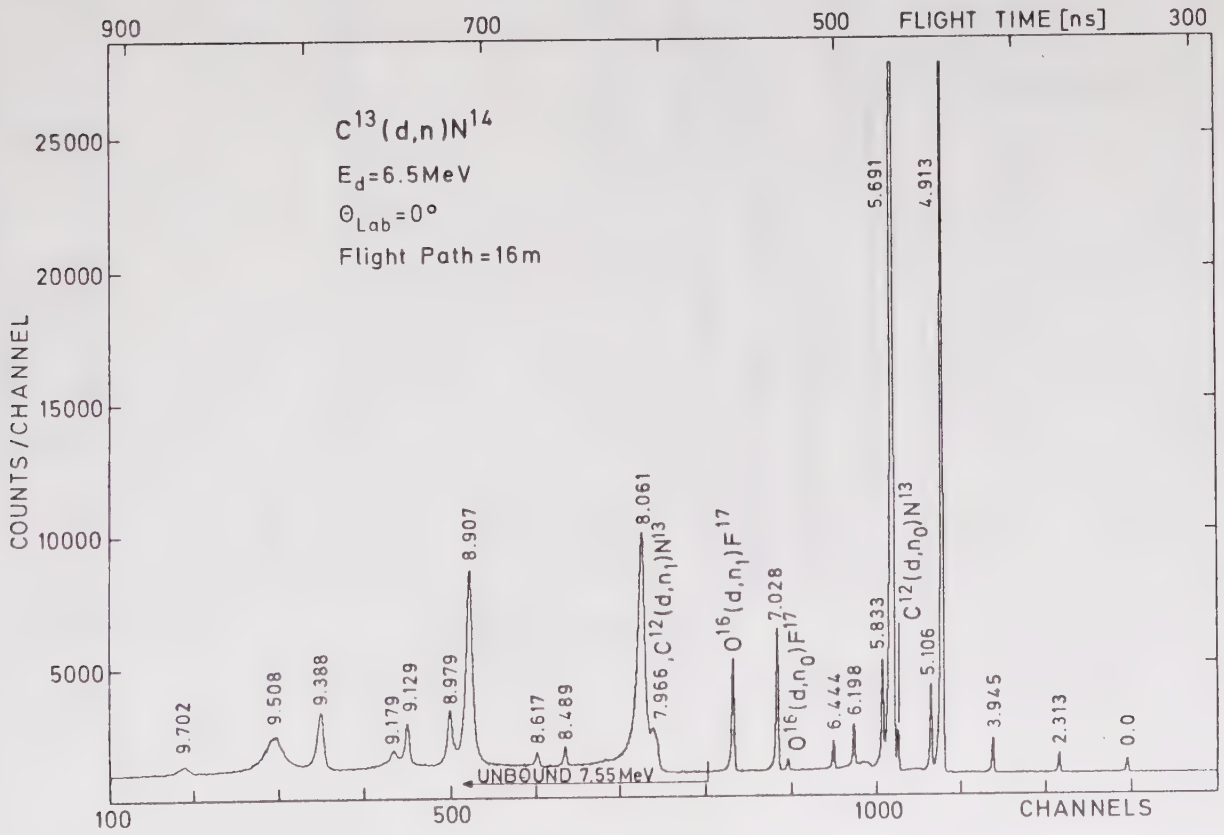

Fig.6 - Time-of-flight spectrum of neutrons from $C^{13}(d,n)N^{14}$ reaction at deuteron energy of E_d = 6.5 MeV .

Fig.7 shows the time-of-flight spectrum at a laboratory angle $\theta_{Lab} = 0^{o}$ for neutron groups from the $C^{14}(d,n)N^{15}$ reaction which leave N^{15} in the ground state and various excited states. The prominent peaks arise from C^{12} and O^{16} contaminants in the target while some less prominent peaks come from the $C^{13}(d,n)N^{14}$ reaction. Inbetween are peaks from the $C^{14}(d,n)N^{15}$ reaction.

The doublet of the first and second excited states at 5.271 and 5.299 MeV is unresolved. The 6.301 MeV state is almost covered by a giant peak arising from the (d,n) reaction on deuterium accumulated in the target from previous use. The unbound region begins at 10.208 MeV excitation energy. Seen at E_x = 11.44 MeV is a new level discovered in this measurement.

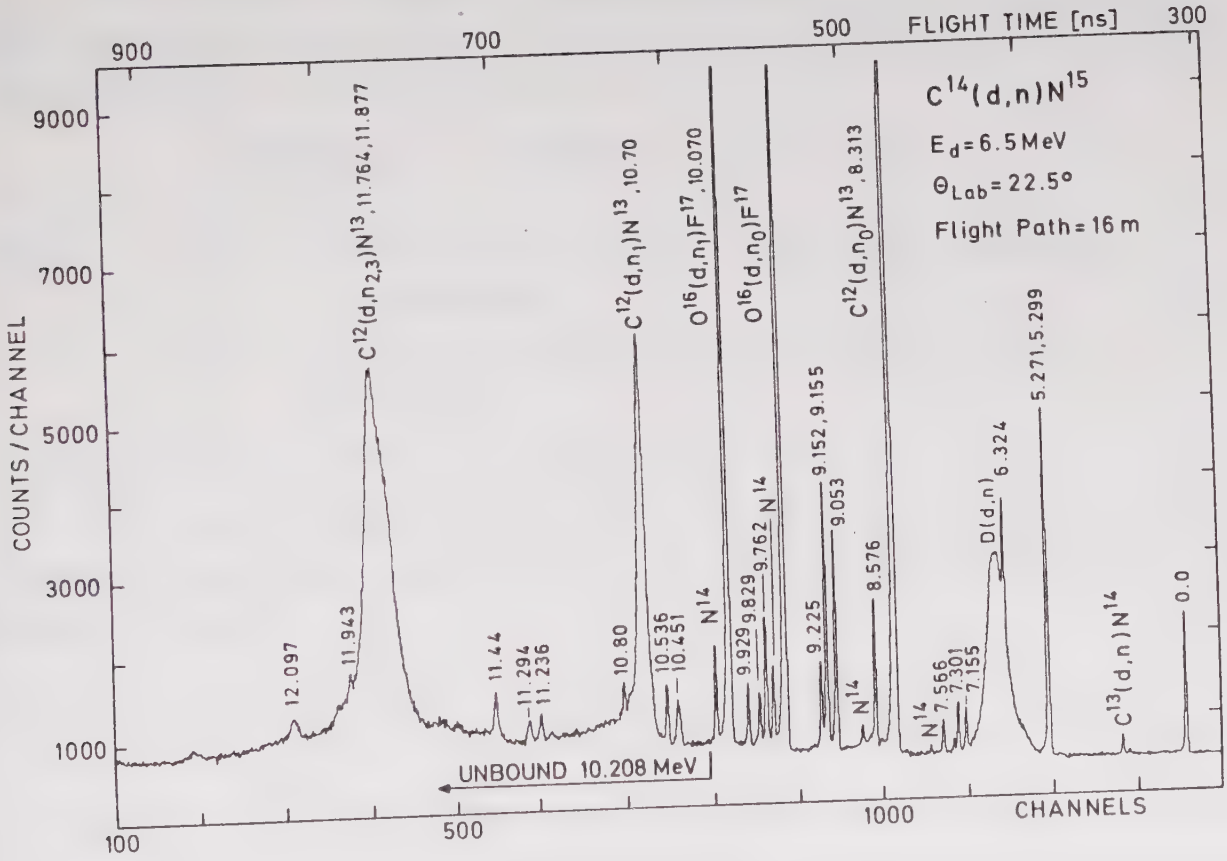

Fig.7 - Time of flight spectrum of neutrons from $C^{14}(d,n)N^{15}$ reaction at deuteron energy of E_d = 6.5 MeV .

4.2 Deduction of Data

4.2.1 Neutron Energy Calibration and Spectra Identification

The neutron energies in the time-of-flight spectrum were calibrated with the help of an auxiliary $Be^9(d,n)B^{10}$ reaction measurement. The well known levels of B^{10} (La66) with their respective neutron energy and flight time, made this reaction a suitable choice within this energy range for the calibration of the neutron time-of-flight spectrometer, and offered a good reference spectrum for the identification of the neutron spectra corresponding to states in $N^{13,14,15}$ from the $C^{12,13,14}(d,n)N^{13,14,15}$ reaction.

The neutron energies E_n were identified with the corresponding excitation energies E_x of the final nucleus through a three step procedure involving Q-value calculations:

$$E_x \xrightarrow{\text{Q-value}} E_n \xrightarrow{(1/2)mv^2} t_n \xrightarrow{\Sigma A_n K^n} K_n$$

where
- t_n - the neutron time-of-flight from target to the detector,
- K_n - the corresponding channel number in the spectrum,
- A_n - constans, where n = 0,1,2,....

The neutron energy E_n in the laboratory system was obtained from the excitation energy E_x through the non-relativistic Q-value equation (Ma68)

$$Q = Q_o - E_x = \frac{M_n + M_f}{M_f} E_n - \frac{M_f - M_d}{M_f} E_d - \frac{2(M_d M_n E_d E_n)^{1/2}}{M_f} \cos\theta_{Lab}. \qquad 4.2.1$$

where
- Q_o - the ground state Q-value of the reaction involved,
- M_n, M_d, M_f - masses of the neutron, deuteron and final nucleus respectively,
- E_n, E_d - energies of the neutron and deuteron, respectively in the laboratory system,
- θ_{Lab} - laboratory angle of the emitted neutron with respect to the incident deuteron (detector angle).

obtained from the law of energy and momentum conservation in nuclear reactions (Ma69).

The neutron flight time t_n was obtained from the neutron energy in the relation

$$E_n(\text{MeV}) = \frac{M_n V_n^2}{2} = (72.29)^2 \{\frac{S(m)}{t(\text{nsec})}\}^2 \qquad 4.2.2$$

with $$t_n(\text{nsec}) = 72.29 \frac{S(m)}{\{E_n(\text{MeV})\}^{1/2}} \qquad 4.2.3$$

where $S(m)$ - flight path (target to detector distance) in units of metre.

The neutron energy was calculated using the Q-value programme.

The flight time t_n was then identified with the corresponding channels in the spectrum through the constants A_o, A_1, A_2, A_3 in the equation

$$t_n = A_o + A_1 K_n + A_2 K_n^2 + A_3 K_n^3 + ... \qquad 4.2.4$$

where $A_2K_n^2$, $A_3K_n^3$, ... - are small corrections for non-linearity of the electronics

$K_n = K_c$ - the channel centroid corresponding to a group of neutrons from the same level.

$$K_c = \frac{\sum_{j=1}^{m} K_j (I_j - I^B)}{\sum_{j=1}^{m} I_j - (K_m - K_1) I^B} \qquad 4.2.5$$

where

I_j - counts in the j-th channel,

I^B - background counts in each channel,

$m = (K_m - K_1)$ - total number of channels under the peak.

The background was obtained from the neighbourhood of the peak concerned using the expression

$$I^B = \frac{1}{2}(I_l^B + I_r^B) \qquad 4.2.6$$

where I_l^B, I_r^B - the backgrounds in the left and right neighbourhood of the peak concerned.

$$I_l^B = \frac{1}{\alpha}\sum_{i_l=1}^{\alpha} I_{i_l} , \quad I_r^B = \frac{1}{\beta}\sum_{i_r=1}^{\beta} I_{i_2} \qquad 4.2.7$$

where

I_{i_l}, I_{i_r} - counts in i_l, and i_r channel in the left and right neighbourhood ,

α, β - the respective total number of channels in the left and right neighbourhood.

The calculation of Eq.4.2.4 for a few well known levels and substitution for the respective channels in the spectrum gave an almost linear time to channel dependence with Eq.4.2.3 which solved the identification of the unknown levels.

4.2.2 Extraction of Experimental Differential Cross-section

The intensities or total counts of the various peaks in the spectrum were extracted using the Tepel programme (Te66) which offers the possibility of fit and separation of overlapping levels. The extracted intensities have the form in the denominator of Eq.4.2.5 and for the various laboratory angles are expressed as

$$I_{Tep}(\theta) = \sum_{j=k}^{m} I_j(\theta, E_n) - (m - k)I^B \qquad 4.2.8$$

which after correction for electronic dead time gives

$$I(\theta) = I_{Tep}(\theta)\frac{Q}{Q_{act}} \qquad 4.2.9$$

where Q - total deuteron charge during measurement

Q_{act} - the active or life charge to which the electronics responded.

With reference to the detector, this intensity corresponds to the original intensity I_o of neutrons from the target incident on the detector surface to give

$$I(\theta) = \varepsilon I_o(\theta) d\Omega_{Lab} \qquad 4.2.10$$

where ε - the detector's efficiency or probability of response,

$d\Omega_{Lab}$ - the solid angle of the detector subtended at the centre of the target,

and

$$d\Omega_{Lab} = \frac{\pi r^2}{S^2} \qquad 4.2.11$$

where r - radius of the detector,

S - detector-to-target distance.

With reference to the target, the reaction rate or neutron intensity corresponds to the cross-section in the expression

$$I_o(\theta) = N_o \rho \sigma(\theta_{Lab}) \qquad 4.2.12$$

where $\sigma(\theta_{Lab}) = \frac{d\sigma}{d\Omega_{Lab}}$ - the differential cross-section of the reaction in (cm^2/sr), $1b = 1 \text{ barn} = 10^{-24} cm^2$.

N_o - the total number of deuterons incident on the target during the measurement time t,

$$N_o = \int \frac{Q dt}{e} \quad , \qquad 4.2.13$$

where e - the fundamental charge = 1.6×10^{-19} Coul.

The nuclear density ρ is the number of nuclei per cm^2 of the target expressed as

$$\rho = \frac{T\,N}{A} \qquad 4.2.14$$

where

T - the target thickness,

N - Avogadro's number = $6.023 \times 10^{23} (Mol^{-1})$,

A - $\frac{\text{Molecular weight of target substance (g/Mol)}}{\text{Number of target nuclei in a molecule of target subs.}}$

Eqs.4.2.10-14 give the differential cross-section in the centre of mass system as

$$\frac{d\sigma}{d\Omega}_{cm}(\theta_{cm}) = \frac{d\sigma}{d\Omega}_{Lab}(\theta_{Lab})\left(\frac{d\Omega_{Lab}}{d\Omega_{cm}}\right) = \frac{I(\theta)A}{\varepsilon N_o T N d\Omega_{Lab}}\left(\frac{d\Omega_{Lab}}{d\Omega_{cm}}\right). \qquad 4.2.15$$

The detector efficiency in the above equation is dependent on the neutron energy, the scintillator's threshold energy, the n-p elastic cross-section, and the thickness of the detector. An approximate expression (Sc60) for liquid scintillator detectors is given as follows

$$\varepsilon(E_n, E_{th}, t) = \text{const.}\,(1 - e^{-n_H \sigma_H t})\left(\frac{E_n - E_{th}}{E_n}\right) \qquad 4.2.16$$

where E_n - the neutron energy,

E_{th} - the threshold energy for the detection of neutrons,

t - the thickness of the scintillator (detector)

n_H - the number of hydrogen atoms per cm^3 of the scintillator, $n_H = 4.86 \times 10^{22} cm^{-3}$ for NE213.

σ_H - the cross-section for neutron-proton elastic scattering (in cm^2),

$\sigma_H \approx \{4.83\, E_n^{-1/2}(MeV) - 0.578\}$ barn (Ma6).

The absolute threshold energy of a detector was obtained by comparison of a particular level in the two equivalent spectra resulting from the upper and lower threshold energy setting of the electronics (Sect.3.4.2). For a particular level in the two identical spectra, Eqs.4.2.15 and 4.2.16 give the relation

$$\frac{I_n^{up}}{I_n^{low}} = \frac{E_n - E_{th}^{up}}{E_n - E_{th}^{low}} \qquad 4.2.17$$

where I_n^{up} - the total counts for a particular level in the upper-threshold spectrum,

I_n^{low} - the total counts for the same level in the lower-threshold spectrum,

E_{th}^{up}, E_{th}^{low} - the corresponding upper and lower threshold energies.

The upper and lower threshold energies of the electronics E_{el}^{up} , E_{el}^{low} were set in the proportion

$$E_{el}^{up} = \alpha E_{el}^{low} \qquad 4.2.18$$

where $\alpha = 2.1$ and $E_{el}^{low} \approx 1.8$ MeV .

The substitution of Eq.4.2.18 into 4.2.17 gives the absolute lower threshold energy of the detectors as

$$E_{th}^{low} = \left(\frac{1 - \kappa}{\alpha - \kappa}\right) E_n \qquad 4.2.19$$

where $$\kappa = \frac{I_n^{up}}{I_n^{low}} \qquad 4.2.20$$

The various values of the absolute threshold energies from Eq.4.2.19 obtained for the different detectors were used in calculating the corresponding efficiencies for the various

neutron energies using the Monte-Carlo programme (Te68, Kl72) since for $E_n \geq 7$ MeV the experimental efficiency (Kl71) deviates appreciably from the approximate expression in Eg.4.2.16 and is better described by the Monte-Carlo calculations.

CHAPTER 5

ANALYSIS OF EXPERIMENTAL DATA

5.1 The Optical-Potential Parameters

To analyse the experimental data, the optical-potential parameters generating the scattering amplitudes in the DI and CN channels (Chapter 2) must be determined in conjunction with experiment. With the DWUCK (Ku67, RÖ70) and LULU (Pi72) programmes, the DWBA and Hauser-Feshbach calculations of Chapter 2 were performed for analysing the experimental data. An incoherent sum of the two in a combination of both programmes into a search procedure OPTIMA (Si72) was used to determine the appropriate potential parameters for the complex optical potential wherein trial parameters were varied until an uptimum fit to the experimental data was acheived. The optical potential used in generating the scattered deuteron and neutron waves in the respective entrance and exit channels as well as that for the bound-state proton has the form shown in Table 5.1.

The surface diffuseness parameter a_s, and the corresponding radius r_{os} in the derivative form could be set equal to that of the Saxon-Woods form factor since calculated cross-sections are very insensitive to the chosen form of g(r). The spin-orbit potential for the bound-state was chosen to be the "Thomas Form Factor" with $\lambda_{so} = 25$. For a given binding energy E_B, the programme matched the potential depth V_o in the Schrödinger equation until a solution for the bound-particle wave function was obtained.

The neutron parameters were taken from Hodgson (Ho71) with the optical potential parameters dependent on the neutron energy, the mass and isospin of the residual nucleus. The deuteron parameters were determined in this work by a systematic search for the

Table 5.1 - The optical potential form.

COMPLEX OPTICAL POTENTIAL

$$V(r) = V_C(r) + V_o f(r) + iW_v g_v(r) + iW_s g_s(r) + V_{so} h(r)\ \vec{l}.\vec{s}$$

COULOMB POTENTIAL

$$V_C(r) = \begin{cases} \dfrac{Z_1 Z_2 e^2}{2R_C}\{3 - (\dfrac{r}{R_C})^2\} & \text{for } r < R_C \\ \dfrac{Z_1 Z_2 e^2}{r} & \text{for } r > R_C\ , \quad R_C = r_{oC} A^{1/3} \end{cases}$$

SAXON - WOODS FORM FACTOR

$$f(r) = \frac{1}{1 + \exp(\frac{r-R}{a})}\ , \quad g_v = \frac{1}{1 + \exp(\frac{r-R_v}{a_v})}\ , \quad R = r_o A^{1/3}$$

SAXON - WOODS DERIVATIVE

$$g_s(r) = \frac{d}{dr} f(r) = \frac{4 \exp(\frac{r-R_s}{a_s})}{\{1 + \exp(\frac{r-R_s}{a_s})\}^2}$$

SPIN - ORBIT DERIVATIVE

$$h(r) = \frac{\hbar^2}{m_\pi^2 c^2} \frac{1}{r} \frac{d}{dr} f(r)$$

BOUND - STATE POTENTIAL FORM

$$V(r) = V_C(r) - V_o f(r) + V_{so} h(r)\ \vec{l}.\vec{s}$$

where
- a - nucleus diffuseness parameter,
- Z_1 - proton number of the incident/emitted particle,
- Z_2 - proton number of the target/residual nucleus,
- m_π - the pion mass,
- V_o - real-cental-potential depth,
- W_v, W_s - imaginary volume/surface potential depth,
- V_{so} - spin-orbit potential.

$C^{14}(d,n)N^{15}$ transition of each l-value using a mean-square-deviation fit. Fig.8 shows the dependence of the mean-square-deviation χ^2 on the real potential V and radius r, for an l = 1 transition, with other parameters fixed. The mean-square-deviation from the experimental data is

$$\chi^2(V,r) = \sum_n \left(\frac{\sigma^{th}(\theta) - \sigma^{exp}(\theta)}{\Delta\sigma^{exp}(\theta)}\right)^2 \qquad 5.1$$

where $\sigma^{th}(\theta)$ - the incoherent sum of the DWBA and and Hauser-Feshbach calculations,

n - the number of experimental points.

In the upper part of Fig.8, each of the curves 1-7 represents the dependence of χ^2 on V with r_o as parameter. It shows a first and second minimum as the potential increases. The lower envelope (7-1) indicates the best fit (3) for all potentials between 45 and 140 MeV, and radii ranging from 0.9 to 1.5 fm with other parameters fixed. The two envelopes being very flat demonstrate the well known continuous ambiquity of the potential parameters (Vr_o^2 = const.). It is also shown clearly in the lower part of Fig.8 by the two curves a and b, which give the position of the minimum in the χ^2-valley in the V,r_o-plane. The existence of two valleys (a,b) is connected with the discrete ambiquity resulting from the equivalence of scattering phase shifts $\delta_\ell + n\pi$, with n = 0, 1, 2,....

The point (d,d) shows the best fit for deuteron elastic scattering as determined by Grabisch (Gr72). The (d,d) parameters were used for the final analysis in this work as they gave a good average fit for transitions of all l-values which can be seen for instance in Fig.9 for the l = 2 transition, where the (d,d) point lies on the Vr_o^2 = const. curve.

That the best fit potential determined from the ground-state transition (Fig.8) deviates from the (d,d) potential is not a serious discrepancy, as the ground state with its large binding energy is connected with a transition amplitude concentrated much more in the nuclear interior than the excited states. In such a case the DWBA is known to be less reliable.

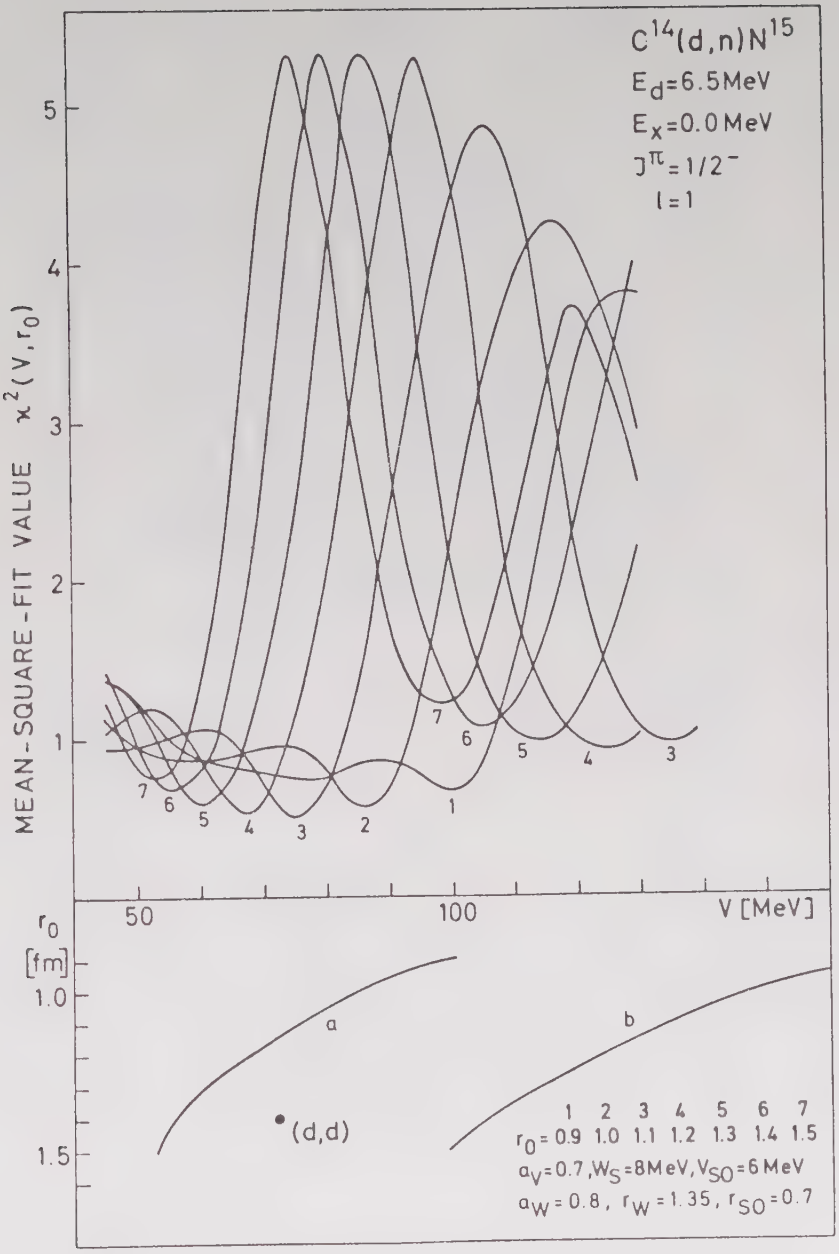

Fig.8 - Dependence of the mean-square-deviation χ^2 on the real potential V_o and radius r, for an l = 1 transition in the $C^{14}(d,n)N^{15}$ reaction.

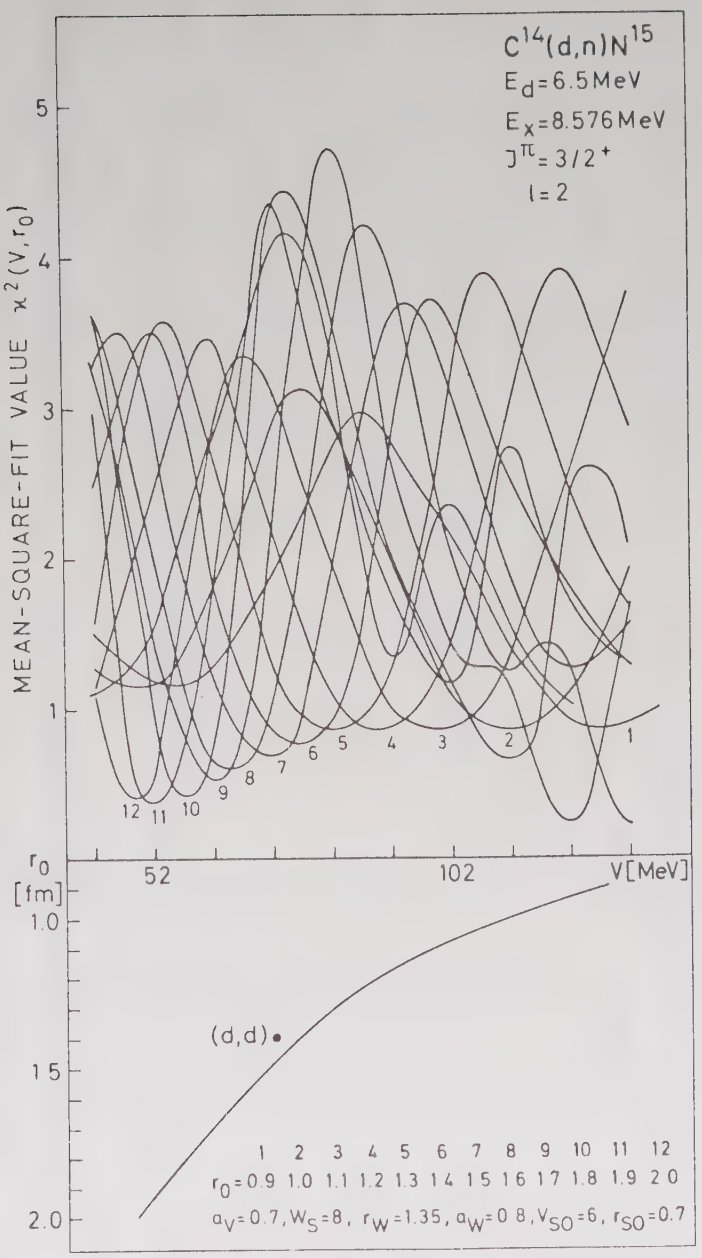

Fig.9 - Dependence of the mean-square-deviation χ^2 on the real potential V_o and radius r for an l = 2 transition in the C^{14}d,n)N^{15} reaction.

Table 5.2 shows the optical-potential parameters used in the final DWBA and Hauser-Feshbach calculations for the $C^{13}(d,n)N^{14}$ and $C^{14}(d,n)N^{15}$ reaction analysis.

Table 5.2 - Potential parameters used in the $C^{13,14}(d,n)N^{14,15}$ reaction analysis.

Reaction channel	Real potential parameters			Imaginary vol. pot.parameters			Imaginary surface pot.parameters			Spin - orbit pot.parameters			Coul. param	Remark
	V_o (Mev)	r_o (fm)	a (fm)	W_v (MeV)	r_v (fm)	a_v (fm)	W_s (MeV)	r_s (fm)	a_s (fm)	V_{so} (Mev)	r_{so} (fm)	a_{so} (fm)	r_C (fm)	
$d + C^{13,14}$	72	1.4	0.7	8.	1.35	0.8				7.5	1.4	0.7	1.3	(a)
$p + C^{13,14}$		1.3	0.65							25	1.35	0.8	1.3	(b)
$n + N^{14,15}$	$56.3-32E_n$ -24η	1.17	0.75				$13-0.25E_n$ -12η	1.26	0.58	12.4	1.01	0.75		(c)

a) Determined in this work and that of Grabisch (Gr72)

b) The trial potential 60 MeV was varied by the programme until a value suiting the given experimental binding energy was obtained.

c) $\eta = \frac{N-Z}{A}$, where N,Z,A, - neutron, proton and mass numbers of the residual nucleus.

5.2 Unbound States Analysis

A direct DWBA calculation method for unbound states was not available. This involves a modification of the bound state calculations in which the bound state wave function ψ_B in the post expression 2.2 is replaced by a positive energy wave function $\psi_B^{(-)}(k_p, r_{pA}, \xi_A)$, an eigenfunction for the system (A + p) in a scattering state. This means replacing the proton radial wave function $\phi_{\ell j}(r)$ in Eq.2.11 by a scattering wave function which no more normalizes. This leads to very slowly convergent oscillating radial integrands in the radial integral 2.11 of an explicit simplified form

$$\int \phi_{L_n, J_n}(k_n, r)\phi_{n\ell j}(k_p, r)\phi_{L_d, J_d}(k_d, r)dr = \int \frac{1}{r} e^{ik_n r} e^{ik_p r} e^{ik_d r} dr \qquad 5.2$$

Fortune et al (Fo70) evaluated these integrals by contour integration in a complex-radius plane setting $r = R + i\rho$ which avoids the computation of wave functions out to large distances required by the Huby-Mines Gaussian damping technique (Hu65).

In this work the unbound states of the $C^{13}(d,n)N^{14}$ and $C^{14}(d,n)N^{15}$ reactions were analysed using an extrapolation method, the only method available at the moment. The extrapolation method, though cumbersome, is in no doubt as effective as the Fortune-Vincent complex-plane integration method in its reproduction of the experimental angular distribution shapes as can be seen in Figs.12,13,16 and 17. In the extrapolation method, DWBA and Hauser-Feshbach calculations were done for particular lj-states in the negative-binding-energy region with the binding energies $E_B = E^p_{th} - E_x$ (E^p_{th} - proton threshold energy) varied towards the positive-energy region. The obtained cross-sections were extrapolated into the positive-binding-energy region and read off for the corresponding lj-states and various angles. Fig.10 shows the result of this indirect calculation for the l = 2 states in the $C^{14}(d,n)N^{15}$ reaction. In Fig.10, the general pattern of the cross-sections shows an increase of DWBA and a decrease of H-F cross-sections in the unbound region. This explains the dominance of direct interactions over compound nucleus reaction in the unbound region. As the unbound region is approached, the direct interaction

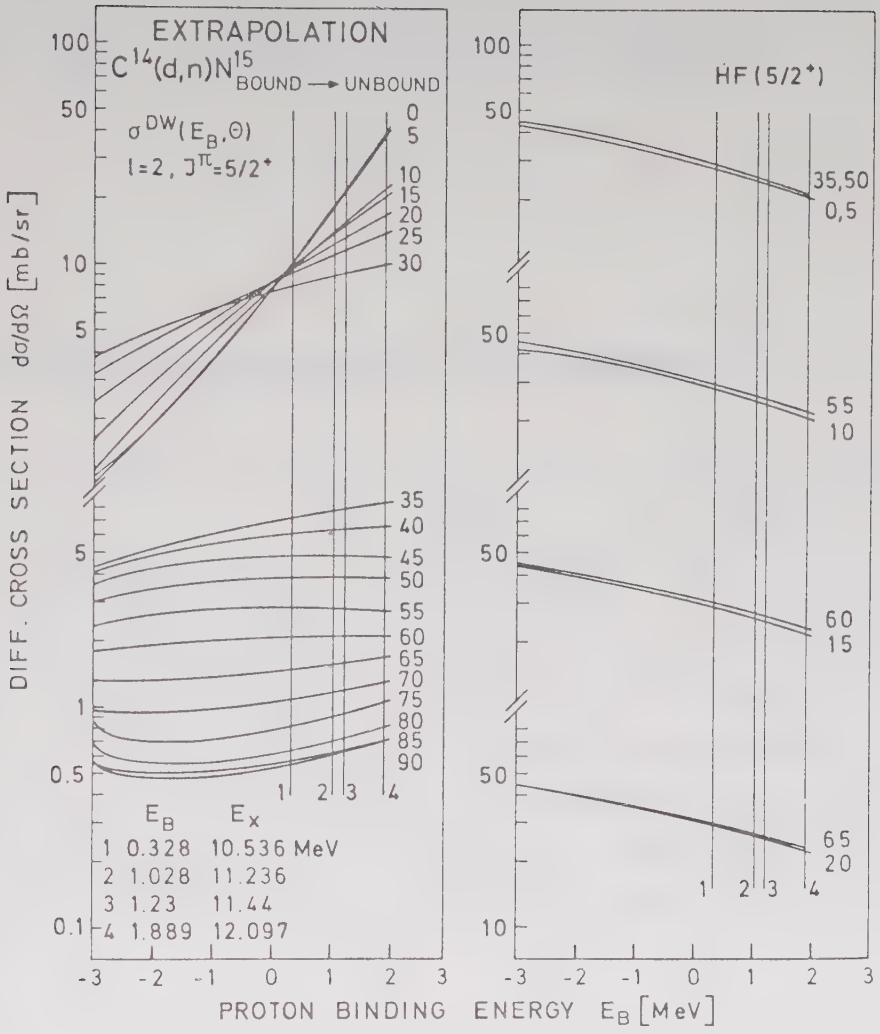

Fig.10 - Extrapolation of DWBA and H-F calculations to unbound region for the l = 2 states in N^{15}. The angle is given as parameter at the right hand side of each curve.

shifts its maximum from about 35^{o} in the negative energy region to the foward direction in the positive energy region. This foward-direction peaking tendency in the positive energy region is characteristic for transitions of all l-values, which shows the effect of nuclear surface interaction at increasing radius $\vec{r}$ and therefore decreasing momentum transfer $\vec{q}$ for the transfer of a given l-value

$$\vec{l} = \vec{r} \times \vec{q} \qquad 5.3$$

5.3 Angular Distribution Fit with DWBA and H-F Calculations

The results of the DWBA and Hauser-Feshbach calculations in comparison with the experimental angular distributions for $C^{13}(d,n)N^{14}$ and $C^{14}(d,n)N^{15}$ stripping into bound and unbound states in N^{14} and N^{15} are shown in Figs.11-17. The experimental results are represented by points with absolute error bars, while the dashed curves represent the DWBA and H-F calculations as indicated in the figures. The thick curves are incoherent sums of the two which should reproduce the experimental points. The various states are identified with the various probable transferred angular momenta l, spins and parities J^{π}, and where necessary with isospin T.

In Fig.14 the cross-section of the doublet first and second excited states at E_x = 5.271 MeV (l = 2) and E_x = 5.299 MeV (l = 0) unresolved in the spectrum of Fig.7, has been here decomposed into an l = 0 and an l = 2 components. The fit confirms the dominant feature of the l = 0 state with marked contributions from the l = 2 transition exhibited by its characteristic first maximum at an angle of about 35 degrees CM. in contrast to the l = 0 second maximum which normaly lies at about 55 degrees CM., as can be seen in case of the 9.053 MeV $2s_{1/2}$ excited state. Similarly the doublet states in N^{15} at 9.152 MeV (l_p = 1) and 9.155 MeV with previously unknown parity (Fig.15) have been separated. The same applies to the T = 0, 8.963 and 8.976 MeV doublet unbound states in N^{14} (Fig.12) which have been decomposed assuming only CN contributions from the former.

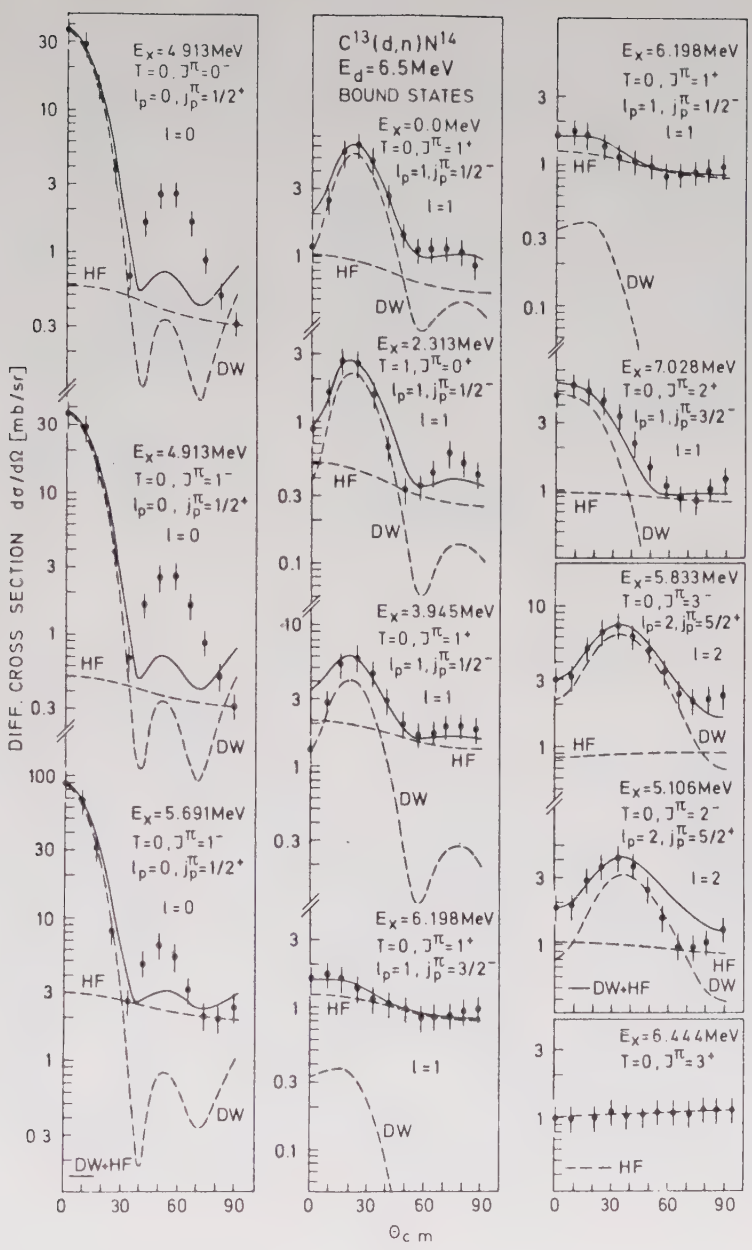

Fig. 11 Experimental and theoretical angular distributions from $C^{13}(d,n)N^{14}$- (bound states) at E_d = 6.5 MeV.

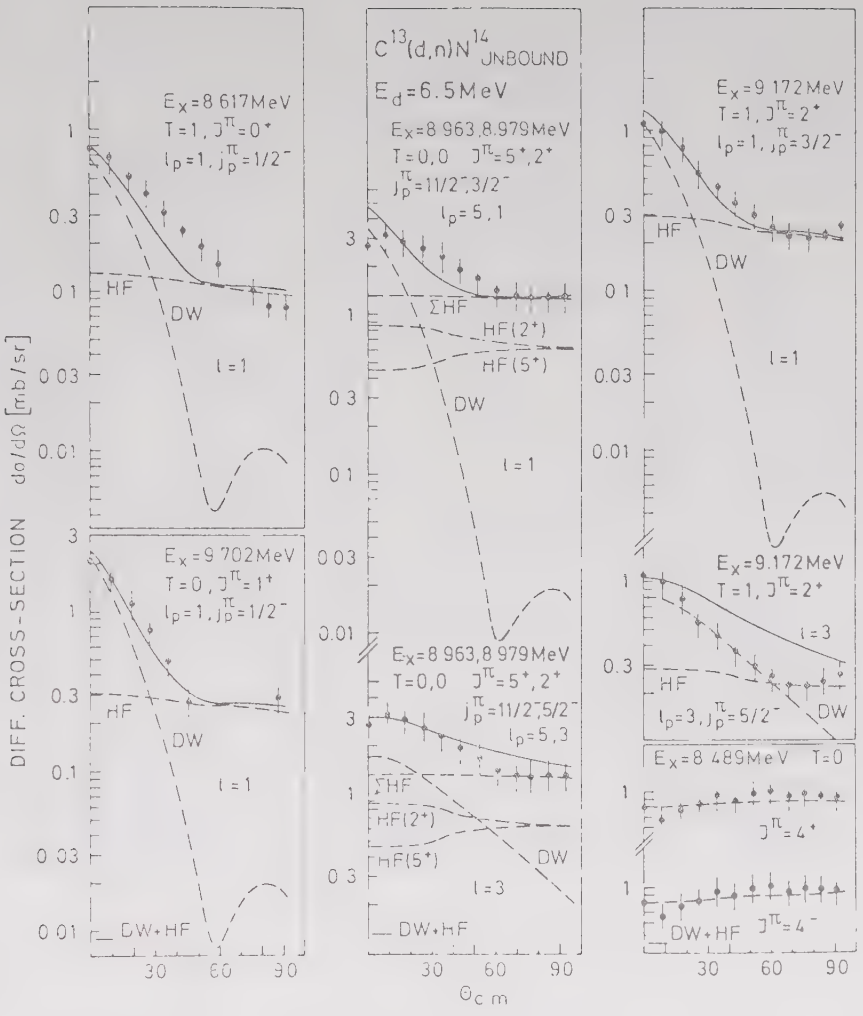

Fig. 12 Experimental and theoretical (extrapolated) angular distributions from $C^{13}(d,n)N^{14}$-(unbound states) at E_d = 6.5 MeV.

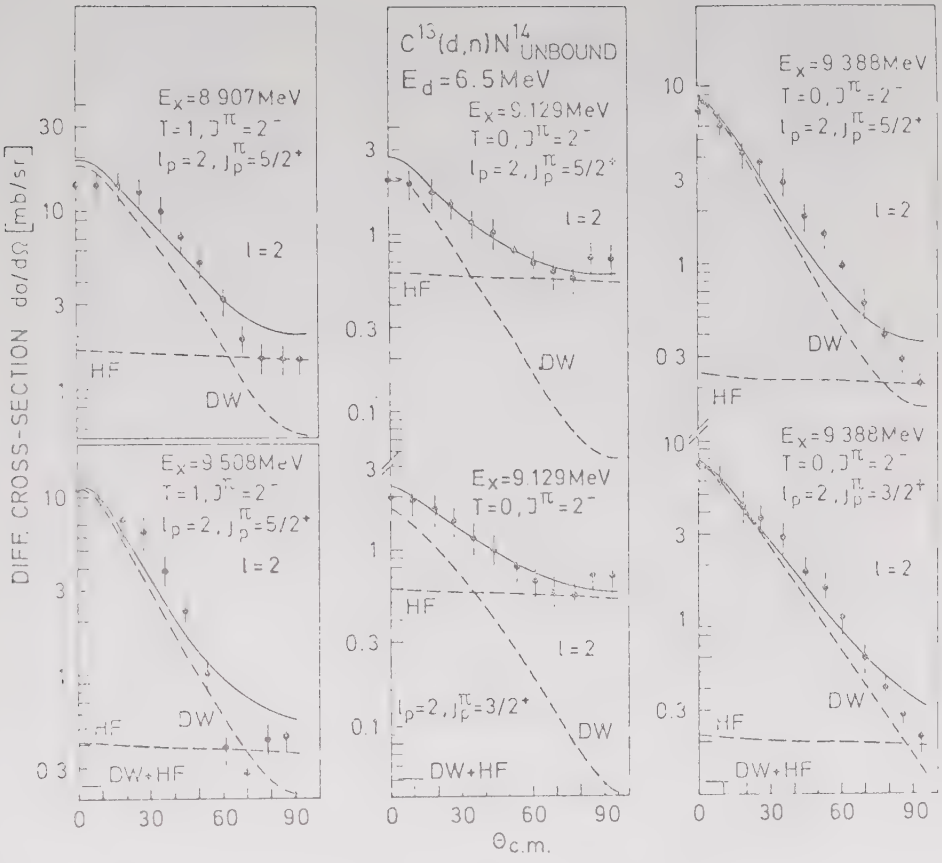

Fig. 13 Experimental and theoretical(extrapolated) angular distributions from $C^{13}(d,n)N^{14}$-(unbound states) at E_d = 6.5 MeV.

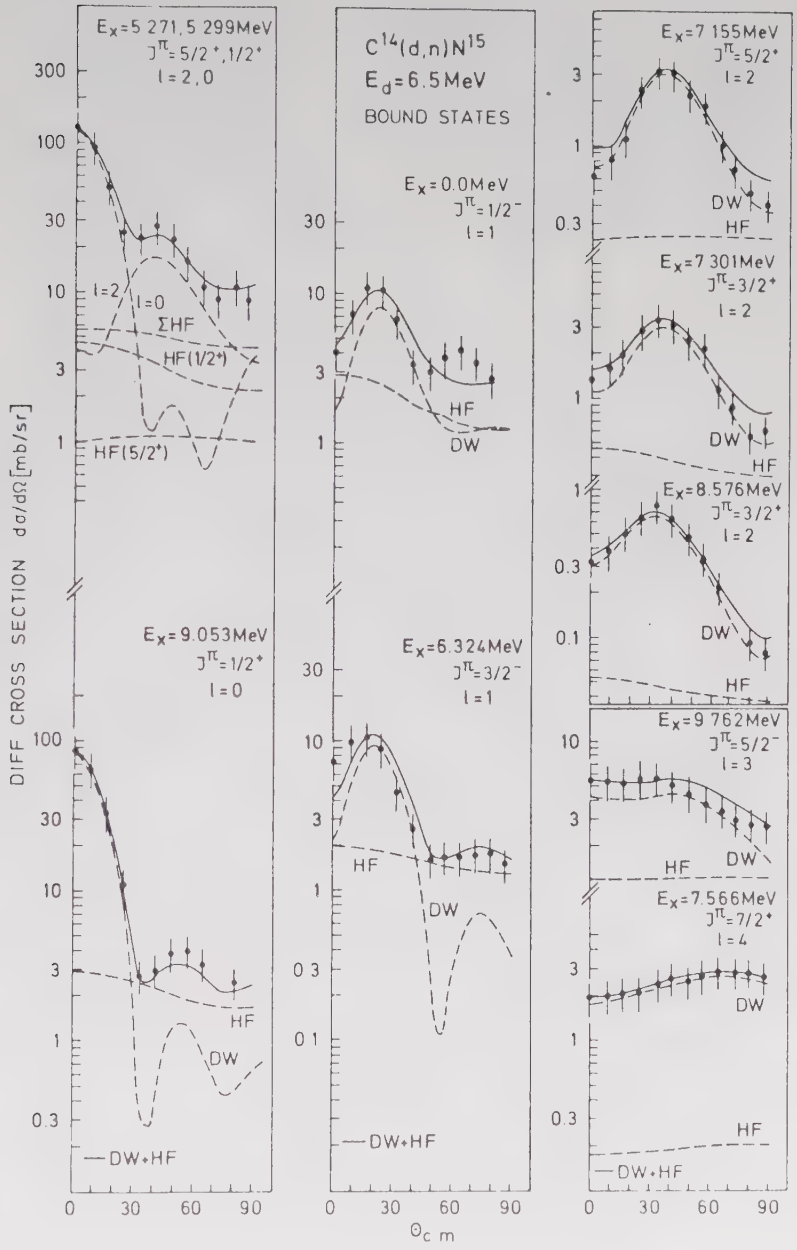

Fig.14 - Experimental and theoretical angular distributions from $C^{14}(d,n)N^{15}$ - (bound states) with previously known spins and parities.
E_d = 6.5 MeV .

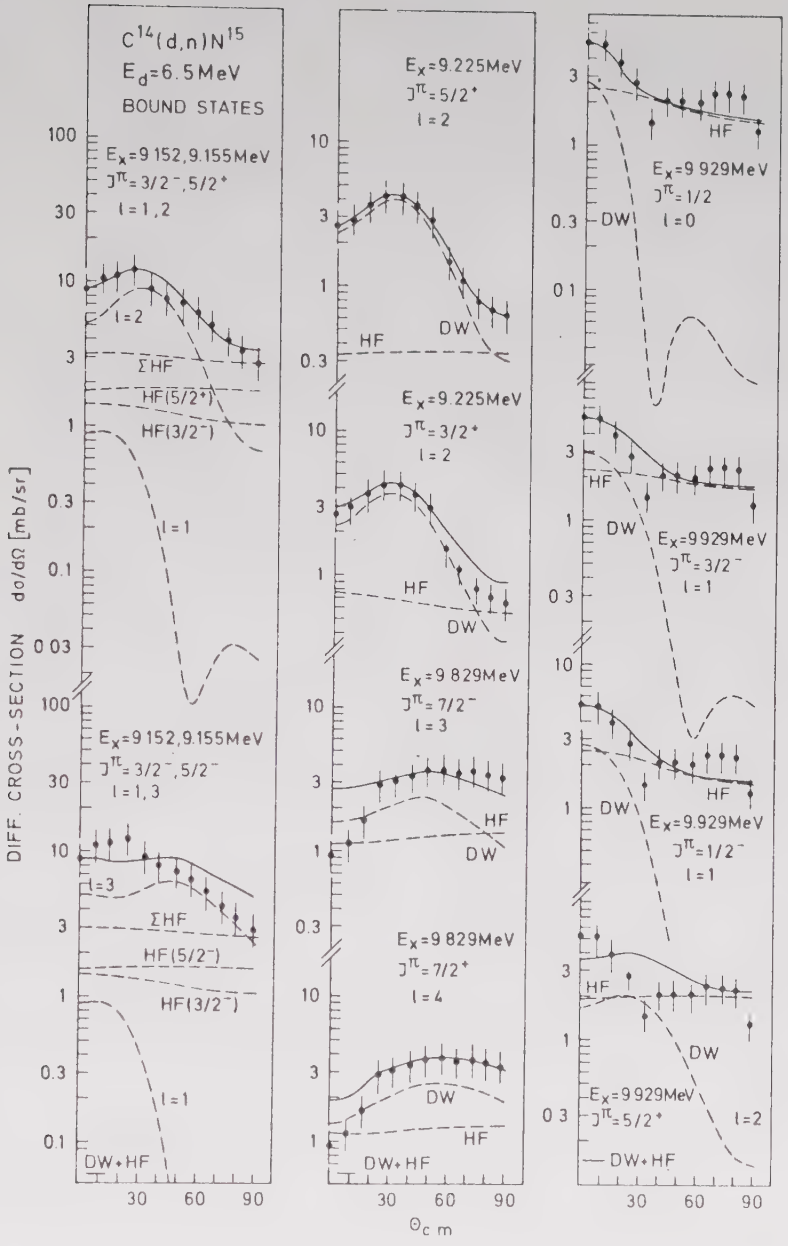

Fig.15 - Experimental and theoretical angular distributions from $C^{14}(d,n)N^{15}$ - (unbound states) with previously unknown spins and parities at E_d = 6.5 MeV .

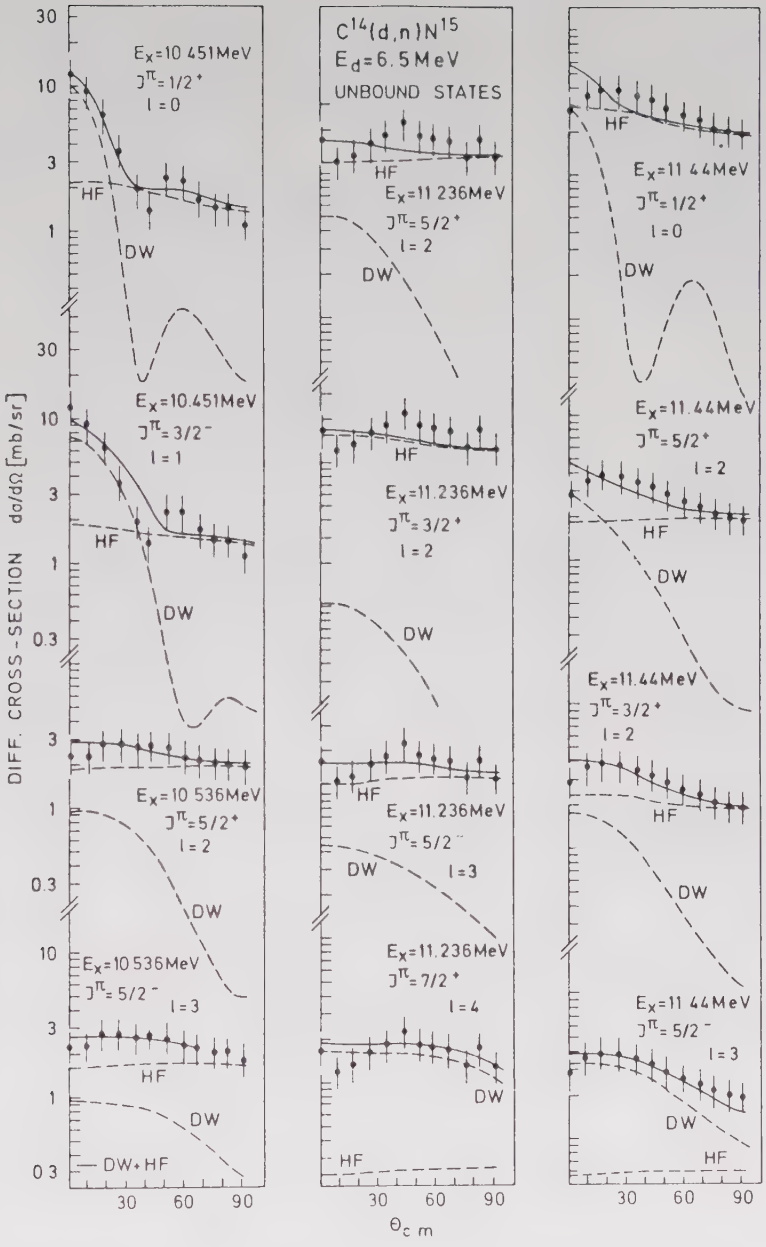

Fig.16 - Experimental and theoretical (extrapolated) angular distributions from $C^{14}(d,n)N^{15}$ - (unbound states) with previously unknown spins and parities at E_d = 6.5 MeV .

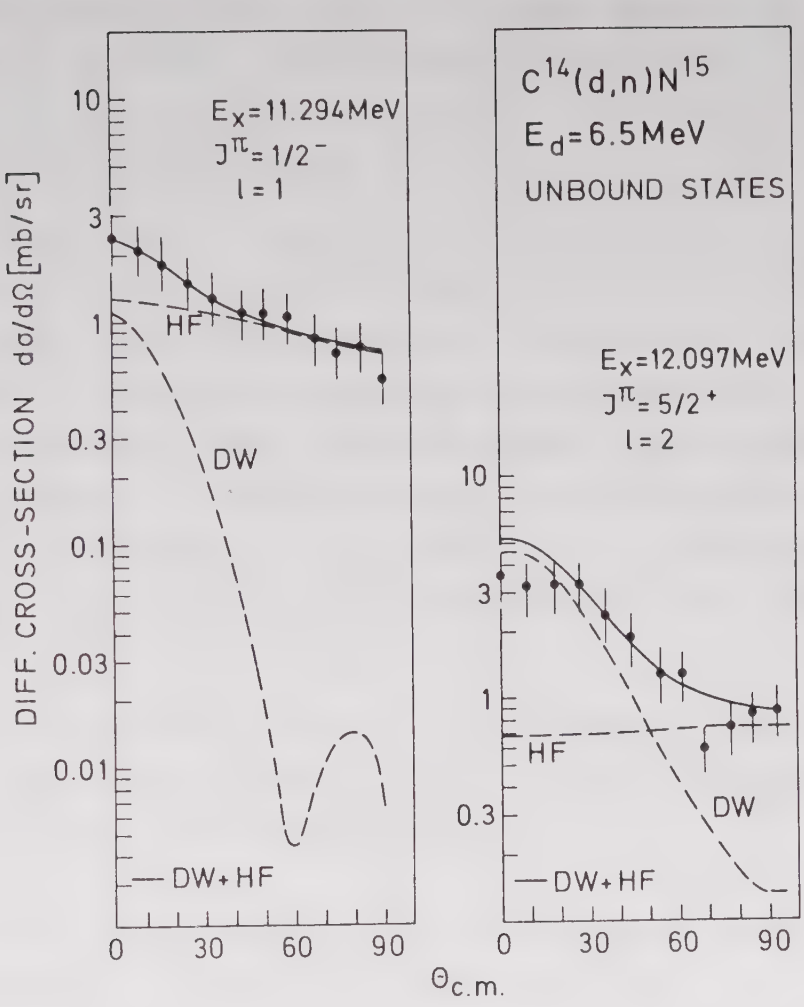

Fig.17 - Experimental and theoretical (extrapolated) angular distributions from $C^{14}(d,n)N^{15}$ (unbound states) with previously known spins and parities at E_d = 6.5 MeV .

On the whole there is a good reproduction of experiment by the DWBA and Hauser-Feshbach calculations except at the second maximum of the $l = 0$ transitions to N^{14} (Fig.11) and the ground state of N^{15} (Fig.14). This is not surprising in the case of the ground state since the bound particle in the ground state sits deep inside the nucleus, the region of which is outside the domain of direct (surface) interaction well described by the DWBA (see also at the end of Sect.5.1). On the other hand the reproduction of the second maximum by theory is not so vital since the fit of the first maximum is more important and sufficient to offer the required spectroscopic information. This also applies for the $l = 0$ transitions to N^{14} where the theory at second maximum shows a deviation of 30 - 50% from experiment. Some states like those with $l = 3$ and $l = 4$ are reproduced by theory only with high or exclusive contributions from Hauser-Feshbach. The goodness of the extrapolation method in reproducing the unbound-states angular distributions is witnessed by the ideal fits of such unbound states with previously known spins and parities like the 11.294 MeV state in N^{15} (Fig.17) and others.

States with prevously unknown spins and/or parities in N^{15} (Figs.15-16) were systematically fitted for various possible J^{π}-values until the best fit was obtained.

The absolute spectroscopic factors extracted from the comparison of theory with experiment in the form

$$S_{\ell j} = \frac{\sigma^{exp}(\theta) - M_{HF}\sigma^{HF}(\theta)}{1.48 \frac{2J_B + 1}{2J_A + 1} C^2 \sigma^{DWBA}_{\ell j}(\theta)} \qquad 5.4$$

are shown in Table 5.3 for the $C^{13}(d,n)N^{14}$ and in Table 5.4 for the $C^{14}(d,n)N^{15}$ stripping reactions.

In Table 5.3 are from left to right the excitation energies E_x of the states in the final nucleus N^{14}; the respective angular momentum l_p and spin-parity j_p^{π} brought in by the transferred proton p; the total spin-parity J^{π} and isospin T of the final states ; the

Table 5.3 Spectroscopic Factors for N^{14} from $C^{13}(d,n)N^{14}$ Stripping Reaction

$E_x(N^{14})$ (MeV)	ℓ_p	j_p^π	J^π	T	Config.	S_{abs}	S_{rel}	M_{HF}
0.0	1	$1/2^-$	1^+	0	$p^2_{1/2}$	1.3	2.02	0.02
2.313	1	$1/2^-$	0^+	1	$p^2_{1/2}$	0.89	1.41	0.02
3.945	1	$1/2^-$	1^+	0	$p^2_{1/2}$	0.37	0.59	0.05
4.913	0	$1/2^+$	0^-	0	$s_{1/2}p_{1/2}$	0.63	1.0	0.05
			1^-			0.21	0.33	0.01
5.106	2	$5/2^+$	2^-	0	$d_{5/2}p_{1/2}$	0.37	0.59	0.02
5.691	0	$1/2^+$	1^-	0	$s_{1/2}p_{1/2}$	0.48	0.76	0.08
5.833	2	$5/2^+$	3^-	0	$d_{5/2}p_{1/2}$	0.46	0.73	0.02
6.198	1	$3/2^-$	1^+	0	$p^{-1}_{3/2}p^{-1}_{1/2}$	0.019	0.03	0.04
		$1/2^-$			$p^2_{1/2}$	0.02	0.032	0.04
6.444	3	$7/2^-$	3^+	0	$f_{7/2}p_{1/2}$			0.03
		$5/2^-$			$f_{5/2}p_{1/2}$			
7.028	1	$3/2^-$	2^+	0	$p^{-1}_{3/2}p^{-1}_{1/2}$	0.02	0.03	0.03
UNBOUND								
8.489	3	$7/2^-$	4^+	0	$f_{7/2}p_{1/2}$			0.04
	4	$9/2^+$	4^-	0	$g_{9/2}p_{1/2}$			0.05
8.617	1	$1/2^-$	0^+	1	$p^2_{1/2}$	0.03	0.05	0.01
8.907	2	$5/2^+$	3^-	1	$d_{5/2}p_{1/2}$	0.03	0.05	0.07
8.963	5	$11/2^-$	5^+	0	$h_{11/2}p_{1/2}$			0.04
8.979	3	$5/2^-$	2^+	0	$f_{5/2}p_{1/2}$	0.02	0.03	0.04
9.129	2	$5/2^+$	2^-	0	$d_{5/2}p_{1/2}$	0.04	0.06	0.03
		$3/2^+$			$d_{3/2}p_{1/2}$	0.03	0.05	0.03
9.172	1	$3/2^-$	2^+	1	$p^{-1}_{3/2}p^{-1}_{1/2}$	0.013	0.02	0.02
9.388	2	$5/2^+$	2^-	0	$d_{5/2}p_{1/2}$	0.09	0.15	0.01
		$3/2^+$			$d_{3/2}p_{1/2}$	0.11	0.17	0.01
9.508	2	$5/2^+$	2^-	1	$d_{5/2}p_{1/2}$	0.12	0.2	0.02
9.702	1	$1/2^-$	1^+	0	$p^2_{1/2}$	0.02	0.03	0.02

Table 5.4: Absolute spectroscopic factors for N^{15} from $C^{14}(d,n)N^{15}$ stripping-reaction.

Spin-parity assignment				Spectroscopic factors	
Ajzenberg-Selove 1970		Present work			
$E_x(N^{15})$ Mev	J^π, T=1/2	l_p	J^π_p	S_{abs}	M_{HF}
0.0	$1/2^-$	1		1.65	0.05
5.271	$5/2^+$	2		0.9	0.02
5.299	$1/2^+$	0		0.58	0.11
6.324	$3/2^-$	1		0.3	0.04
7.155	$5/2^+$	2		0.13	0.01
7.301	$3/2^+$	2		0.18	0.01
7.566	$7/2^+$	4		0.76	0.01
8.576	$3/2^+$	2		0.03	0.001
9.053	$1/2^+$	0		0.3	0.11
9.152	$3/2^-$	1		0.01	0.04
9.155	(5/2)	2	$5/2^+$	0.23	0.05
9.225	$\leq 5/2$	2	$5/2^+$	0.11	0.01
			$3/2^+$	0.15	0.02
9.762	$5/2^-$	3		0.55	0.04
9.829	7/2	4	$7/2^+$	0.61	0.04
9.929	$(1/2,3/2)^+$	0	$1/2^+$	0.02	0.11
Unbound					
10.451	$3/2 \rightarrow 7/2$	0	$1/2^+$	0.08	0.11
10.536	$5/2^{(+)}$	2	$5/2^+$	0.05	0.07
		3	$5/2^-$	0.08	0.06
11.236	$\geq 3/2$	2	$5/2^+$	$\leq$ 0.01	0.05
			$3/2^+$	$\leq$ 0.01	0.06
		3	$5/2^-$	0.03	0.05
		4	$7/2^+$	0.36	0.01
11.294	$1/2^-$	1		0.03	0.07
11.44		2	$3/2^+$	0.09	0.02
		3	$5/2^-$	0.22	0.02
12.097	$5/2^+$	2		0.05	0.04

shell model two-particle configuration of each state; the absolute spectroscopic factors S_{abs} , normalized to the 4.913 MeV (T = 0, $J^{\pi} = 0^{-}$) state to give the relative spectroscopic factors S_{rel} , and finally the Hauser-Feshbach normalization or reduction factor M_{HF} .

In Table 5.4 the first two columns represent the energy states in N^{15} with the respective previous spin-parity assignments as given by Ajzenberg-Selove (Aj70). Here is seen that only the few lower states in N^{15} have been unambiguously identified with spin and parity. The next four columns represent the l-value and spin-parity identifications in this work, the extracted absolute spectroscopic factors S_{abs} , and the Hauser-Feshbach normalization constants M_{HF} .

The normalization factor M_{HF} is seen in Tables 5.3-4 not to be constant as expected by simple theory assuming the absence of all other reaction channels except the compound reaction. However, M_{HF} must not necessarily be constant since the effect of direct interaction is to remove flux from, or prevent events to go through, the compound channel thus reducing the normalization constant M_{HF} . Moreover, the direct-interaction intensity or cross-section varies for various states such that experimentally the normalization factor M_{HF} decreases with increasing direct-interaction cross-section σ_{DI} . Bobbitt et al. (Bo73) in their study of N^{14} using $C^{13}(d,n)N^{14}$ reaction also found that M_{HF} is not constant.

CHAPTER 6

DISCUSSION

6.1 New Spin and Parity Information

The results of this work consists of new l-values leading to new spin-parity information, and a series of spectroscopic factors.

For all states in N^{14} and N^{15} with already known spin and parity J^{π} , the l-values determined in this work are compatible with such information. The angular distributions of Figs.11-17 are arranged in orders of l-values.

6.1.1 The $C^{13}(d,n)N^{14}$ Reaction

The l-values determined for the bound states in N^{14} (Fi.13) are in general agreement with those of Bobbitt et al (Bo73) except the following new findings.

The 6.198 MeV state ($J^{\pi}=1^{+}$, T=0) identified in the above work to be isotropic and treated with CN mechanism only, has been here identified to be populated via $l_p = 1$ proton transfer as exhibited by the angular distribution.

The 6.444 MeV state ($J^{\pi}=3^{+}$, T=0) angular distribution here displays an isotropic nature and has been treated with coumpound mechanism only, calculated for $J^{\pi}=3^{+}$. This final state spin is not compatible with the $l_p = 1$ transfer assigned by Bobbitt et al.

The unbound states (Figs.12-13) offer new information on spin and parity.

The 8.617 MeV state ($J^{\pi}=0^{+}$, T=1) exhibits an $l_p = 1$ proton transfer as expected, but contrary to the findings of Bobbitt et al.

that it be populated through $l_p = 0$. Of course Bobbitt et al. artificially bounded the unbound states by 50 keV in order to derive l-transfers, and consequently their l-values might not be so reliable as those determined here.

The 8.979 MeV state ($J^\pi=2^+$, T=0) decomposed from the 8.963 MeV ($J^\pi=5^+$) state is here found to display an $l_p = 3$ proton transfer which confirms for the first time one of the theoretical assignments (Ta60, Tr63, Wa60) of $l_p = 1$ or 3.

The 9.172 MeV state ($J^\pi=2^+$, T=1) shows a strong $l_p = 1$ stripping pattern , the same as the 9.702 MeV ($J^\pi=1^+$, T=0) state.

The 8.907, 9.129, 9.388 and 9.508 MeV states (Fig.13) all exhibit prominent $l_p = 2$ proton transfer in the angular distribution through the neutron yield.

These determined l-values confirm for the first time through proton transfer on C^{13} the theoretical spin-parity assignments (Ta60, Tr63, Wa60) for states above 8.907 MeV excitation energy.

6.1.2 The $C^{14}(d,n)N^{15}$ Reaction

For the few lower states in N^{15} (Fi.14) the l-values determined in this work agree very well with the already known spins and parities of these states (Aj70, Al69, La67, Mu67).

New informations on spin and parity are portrayed in Figs.15-16 showing angular distributions for some states whose l-values were previously not known (Aj70) or spins and parities ambiguously assigned.

The 9.155 MeV, J = (5/2) state:

This state with previously unknown parity is not resolved from the 9.152 MeV state with known $J^\pi = 3/2^-$, necessarily populated with $l_p = 1$. To describe the combined angular distribution, an additional $l_p = 2$ component is required for the 9.155 Mev level, the parity of which thus must be positive. The trial fit beneath

it (Fig.15) excludes this state from arising from any other l-transfer except the $l_p = 2$.

The 9.225 MeV, $J \leq 5/2$ state :

This state assigned with undefined spin and parity has been here found to be populated via $l_p = 2$ proton transfer leading to $J^\pi = (3/2, 5/2)^+$. Thus it has a positive parity which is in contradiction to the theoretical $J^\pi = 1/2^-$ negative parity assignment by Lie and Engeland (Li71).

The 9.829 MeV, $J = 7/2$ state:

The angular distribution of this level, also assigned with undefined parity, favours a positive parity $l_p = 4$ proton transfer.

The 9.929 MeV, $J^\pi = (1/2, 3/2)^+$ state:

This state is very controversial. Contrary to the positive parity assignment in Ajzenberg-Selove (Aj70), Mairle and Wagner (Ma73) have identified this state through $O^{16}(d,He^3)N^{15}$ reaction to be of negative parity with $J^\pi = (1/2, 3/2)^-$. Here in this work it is found to have positive parity, populated through $l_p = 0$ proton transfer with definite spin $J^\pi = 1/2^-$. This is convincing when one takes note of the position of the minima in the theoretical and experimental angular distributions of this state in Fig.15, bearing in mind that the error bars are absolute, while the relative errors are smaller than the point size. Hence the shape is unambiguous for an $l_p = 0$ transfer.

The 10.451 MeV, $J^\pi = 3/2 \rightarrow 7/2$ state:

The angular distribution of this state with a wide range of possible spin assignments and unknown parity has been determined in this work to favour positive parity with $l_p = 0$ proton transfer. Here again the position of the minima in the theoretical and experimental angular distributions, the unambiguous shape, and the small relative errors (Fig.16) are convincing enough to assign this state with a positive parity, $l_p = 0$, $J^\pi = 1/2^+$. If at all it is of negative parity ($l_p = 1$), certainly $l_p < 2$ and consequently $J \leq 3/2$. This rules out the theoretical prediction of $J^\pi = 9/2^+$ by Lie and Engeland (Li71).

The 10.536 MeV, $J^{\pi} = 5/2^{(+)}$ state:

This state assigned with uncertainty in parity has been here observed to favour through its angular distribution a negative parity with $l_p = 3$ proton transfer , though the possibility of positive parity cannot be ruled out.

The 11.236 MeV, $J^{\pi} \geq 3/2$ state:

This state remains undecided as regards spin and parity though it seems to be populated through an $l_p = 4$ proton transfer in the neutron yield.

The 11.44 MeV state:

This state is qualified to be a new state discovered in this work since certainly its width Γ is much smaller than the 40 keV width given in Ajzenberg-Selove (Aj70) for an 11.438 MeV, $J^{\pi} = 1/2^{+}$ state at this position. The angular distribution of the neutron yield from this state is in favour of an $l_p = 3$ proton transfer, though $l_p = 2$ may not be totally excluded. Hence $l_p = 2, 3$ with $J^{\pi} = 3/2^{+}, 5/2^{-}$ respectively , are proposed.

6.2 The Spectroscopic Factors

The series of spectroscopic information obtained for $N^{14,15}$ from the $C^{13,14}(d,n)N^{14,15}$ reactions are included in Tables 6.1-2. A glance at the theoretical values of the spectroscopic factors for the ground states is offered by the sum rule (Fr61)

$$\sum \frac{2J_B + 1}{2J_A + 1} C^2 S_{\ell j} = h_p - \frac{h_n}{2T + 1} \qquad 6.2.1$$

where h_p , h_n - the number of proton and neutron holes in the target nucleus,

T - the isospin of the target nucleus.

Asumming pure shell model configurations, the ground state transitions carry the total $l = 1$ ($p_{1/2}$) strength, and applying

equation 6.2.1 gives

$$S_{gs} = 1.5 \qquad \text{for } N^{14,15} \text{ ground states.}$$

This gives an estimate of the values of the ground state spectroscopic factors.

In terms of wave functions, the major configurations or simplest wave function of say the C^{14} required to explain all available stripping measurements is

$$\Psi(C^{14}_{gs}) = \alpha_o (1p_{3/2})^8 (1p_{1/2})^2_{\substack{J^\pi = 0^+ \\ T = 1}} + \alpha_1 (1p_{3/2})^6_{\substack{0^+ \\ 1}} (1p_{1/2})^4$$

$$+ \alpha_2 (1p_{3/2})^8 (2s_{1/2})^2_{\substack{0^+ \\ 1}} + \alpha_3 (1p_{3/2})^8 (1d_{5/2})^2_{\substack{0^+ \\ 1}} \qquad 6.2.2$$

with minor contributions from the $(1p_{3/2})^{-2}$, $(2s_{1/2})^2$, and $(1d_{5/2})^2$ for the ground state (Sh55, Vi57, Ja54, Co67, Au55). Here α_i are the amplitudes of the major components ($\Sigma\alpha_i = 1$).

Assuming the N^{15} ground state to be largely

$$\Psi(N^{15}_{gs}) = (1p_{3/2})^8 (1p_{1/2})^3_{\substack{J^\pi = 1/2^- \\ T = 1/2}} \qquad 6.2.3$$

the overlap between the initial and final system

$$\left\langle C^{14}_{gs} \otimes p_{1/2} | N^{15}_{gs} \right\rangle = \alpha_o \qquad 6.2.4$$

gives the spectroscopic information for the ground state transition

$$S_{gs} = |\alpha_o|^2 \times 1.5 \qquad 6.2.5$$

where α_o^2 can be termed as the reduced width or fraction of the time the C^{14} nucleus spends in the $(p_{3/2})^8 (p_{1/2})^2$ configuration.

Similar wave functions can be constructed for the excited states whose configurations are explained in the next section, to give the theoretical spectroscopic factors of the various states. These factors for the lowest states in N^{15} were calculated using the shell model wave functions of Halbert (Ha57) for the positive parity states, and those of Zuker et al (Zu69). Those for N^{14} were taken from the work of Bobbitt et al (Bo73) based on the shell model calculations of Cohen and Kurath (Co67) for the negative parity states, and those of Sebe Se63) for the positive parity states.

6.2.1 Comparison of Spectroscopic Factors with Previous Measurements and Theory

In comparison with previous experiments and theory, Table 6.1-2 reveal the series of new spectroscopic information on N^{14} which has not existed beyond 8.907 MeV excitation energy. Table 6.1 represent the bound states spectroscopic factors, while Table 6.2 shows the comparison for the unbound states with the only available works of Bobbitt, Fortune, et al.

There is an overall agreement between the experimental and theoretical S-factors except for some bound states for which the experimental S-values are short of the theory by a factor of about 2. There is also a general agreement with the most recent work of Bobbitt et al. The disparity in the quoted absolute S-factors reflects the fact that direct reaction predictions are highly dependent on the choice of the optical potential in this mass region, and that most previous studies fail to account for CN contributions to the reaction cross-sections which is more important in the analysis of (d,n) studies usually undertaken at lower bombarding energies than in the analagous (He^3,d) reactions. The S-factor discrepancy between (d,n) and (He^3,d) is discussed more in Sect.6.2.2.

For the lowest states in N^{15}, Table 6.3 shows the comparison of the absolute spectroscopic factors with previous experiments and theory. To give an insight into the configuration and strength

Table 6.1 - Bound-states spectroscopic factors for N^{14} compared with previous measurements and theory

					This work			Previous measurements							Theory	
Type of reaction					(d, n)			(d, n)		(d,n)	(d,n)	(d,n)	(d,n)	(He^3,d)	jj-	
Projectiles energy					6.5			4.5,5.,5.5		11.8	6.0	6.0	7.0	15.0	shell	Co67
Reference								Bo73		Mu71	Fu66	Fu67	Co68	Ho69	Model	Se63
$E_x(N^{14})$ (MeV)	l_p	j^π	J^π	T	S_{abs}	S_{rel}	M_{HF}	S_{abs}	M_{HF}	S_{abs}	S_{rel}	S_{rel}	S_{rel}	S_{abs}	S_{th}	S_{th}
0.0	1	$1/2^-$	1^+	0	1.3	2.02	0.02	1.0	0.22	2.18	0.72	0.95	0.72	1.07	2	1.39
2.313	1	$1/2^-$	0^+	1	0.89	1.41	0.02	0.97	0.26	2.48	0.89	1.09	0.53	1.64	2	1.73
3.945	1	$1/2^-$	1^+	0	0.37	0.59	0.05	0.38	0.19	0.82	0.44	0.54	0.28	0.42	0	0.4
			0^-		0.63	1.00	0.01	0.70	0.03		1.00	1.00	1.00	1.00	1	0.99
4.913	0	$1/2^+$		0												
			1^-		0.21	0.33	0.02									
5.106	2	$5/2^+$	2^-	0	0.37	0.59	0.02	0.67	0.28		1.11	1.20	0.79	0.83	1	0.94
5.961	0	$1/2^+$	1^-	0	0.48	0.76	0.08	0.79	0.10		1.01	0.99	0.63	0.91	1	0.80
5.833	2	$5/2^+$	3^-	0	0.46	0.73	0.02	0.87	0.39		0.94	0.98	0.68	0.55	1	0.82
		$3/2^-$			0.019	0.03	0.04									
6.198	1		1^+	0					1.00				0.12	0.03		
		$1/2^-$			0.02	0.03										
6.444	3		3^+	0			0.03		0.49					0.04		
7.028	1	$3/2^-$	2^+	0	0.02	0.03	0.03	0.23	0.33		0.06	0.07	0.12	0.13		0.13
7.966	1		$2^{(+)}$	0				0.12	0.20							
8.061	1		1^-	1				0.74	0.43		1.20					

Table 6.2 - Unbound-states spectroscopic factors for N^{14} compared with previous measurements. (Theory not available).

					This work			Previous work		
Type of reaction					(d,n)			(d,n)		(He^3,d)
Projectiles energy (MeV)					6.5			4.5, 5., 5.5		15.0
Reference								Bo73		Fo71
$E_x(N^{14})$ (MeV)	l_p	j^π	J^π	T	S_{abs}	S_{rel}	M_{HF}	S_{abs}	M_{HF}	S_{abs}
	3	$7/2^-$	4^+	0			0.04	0.18	0.00	<0.07
8.489	4	$9/2^+$	4^-	0			0.05			
8.617	1	$1/2^+$	0^+	1	0.03	0.05	0.01	0.10	0.00	<0.24
8.80	1		0^-	1						
8.907	2	$5/2^+$	3^-	1	0.03	0.05	0.07	0.6	0.00	0.72
8.963	5	$11/2^-$	5^+	0			0.04			
8.979	3	$5/2^-$	2^+	0	0.02	0.03	0.04			
		$5/2^+$			0.04	0.06	0.03			
9.129	2		2^-	0						
		$3/2^+$			0.03	0.05	0.03			
9.172	1	$3/2^-$	2^+	1	0.013	0.02	0.02			
		$5/2^+$			0.09	0.19	0.01			
9.388	2		2^-	0						
		$3/2^+$			0.11	0.17	0.01			
9.508	2	$5/2^+$	2^-	1	0.12	0.2	0.02			
9.702	1	$1/2^-$	1^+	0	0.02	0.03	0.02			

of the various states, Fig.18 shows the absolute spectroscopic factors for the lowest states in N^{15} in comparison with those of its mirror nucleus O^{15} obtained from $N^{14}(d,n)O^{15}$ reaction also measured here previously (Bo71).

In Fig.18, the absolute experimental spectroscopic factors S are represented by thick horizontal bars to the negative direction for N^{15}, and by dashed horizontal bars to the right for O^{15}. The same holds for their respective theoretical spectroscopic factors based on the shell model calculations of Halbert or Zuker.

Table 6.3 - Spectroscopic factors for the lowest states in N^{15} compared with previous measurements and theory.

Ajzenberg-Selove '70		Present work				Previous measurements		Theory		
		Reaction type		(d, n)		(d,n)	(He^3,d)			Pure jj-coupling
		Projectiles energy (MeV)		6.5		3.09	14.0	Halbert	Zuker	
		Reference				La67	Al69	Ha57	Zu69	
$E_x(N^{15})$ (MeV)	J^π	l_p	Configuration	S_{abs}	M_{HF}	S_{abs}	S_{rel}	S_{th}	S_{th}	S_{th}
0.0	$1/2^-$	1	$(p_{1/2})^3$	1.65	0.05	1.70	2.00	1.5	1.5	1.5
5.271	$5/2^+$	2	$(p_{1/2})^2_0(d_{5/2})^1$	0.9	0.02		1.00	0.74	0.5	1.0
5.299	$1/2^+$	0	$(p_{1/2})^2_0(s_{1/2})^1$	0.58	0.11	0.62	0.68	0.51	0.33	1.0
6.324	$3/2^-$	1	$(p_{1/2})^4_0(p_{3/2})^{-1}$	0.3	0.04	0.56	0.14			0.0
7.155	$5/2^+$	2	$(p_{1/2})^2_1(d_{5/2})^1$	0.13	0.01			0.05	0.01	0.0
7.301	$3/2^+$	2	$(p_{1/2})^2_1(s_{1/2})^1$	0.18	0.01			0.03		0.0
7.566	$7/2^+$	4	$(p_{1/2})^2_1(d_{5/2})^1$	0.76	0.01					
8.576	$3/2^+$	2	$(p_{1/2})^2_1(d_{5/2})^1$	0.03	0.00			0.04		0.00
9.053	$1/2^+$	0	$(p_{1/2})^2_1(s_{1/2})^1$	0.3	0.11	0.28		0.08	0.31	0.0

a) In these calculations, the target-ground state is assumed to be pure $(p_{3/2})^8(p_{1/2})^2$.

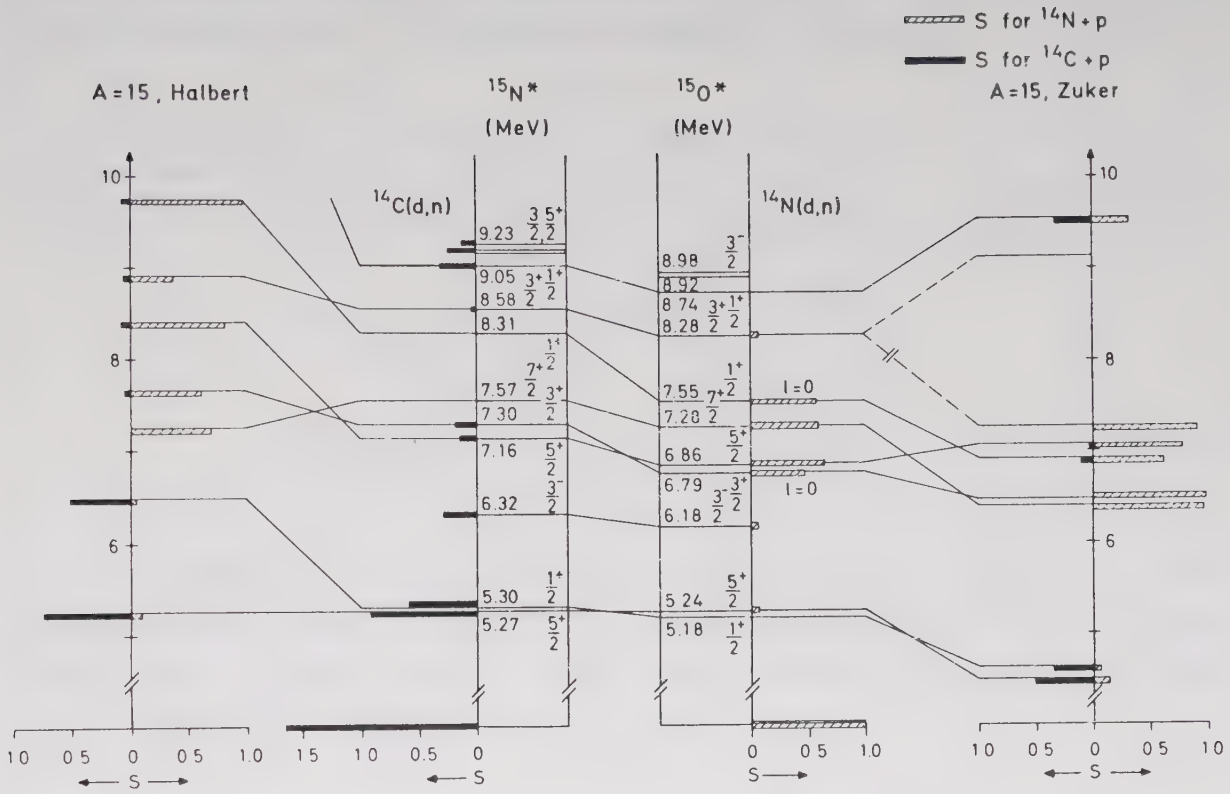

Fig.18 - Comparison of absolute S-factors of the lowest analog states in the mirror nuclei N^{15} and O^{15} with theory.

Experimentally, the spectroscopic factors for N^{15} and O^{15} show

1) two states, strong in $C^{14}(d,n)N^{15}$, but weak in $N^{14}(d,n)O^{15}$ reaction,
2) four states, strong in $N^{14}(d,n)O^{15}$, but weak in $C^{14}(d,n)N^{15}$ reaction.

Fig.19 offers in pure jj-coupling a picture of a simple qualitative explanation of these phenomina as follows.

The lowest states with positive parity (π = +) in A = 15 nuclei are formed by the coupling of a $2s_{1/2}$ or $1d_{1/2}$ nucleon to the A = 14 system whose ground state has the configuration

$$(1p_{1/2})^2_{0^+} \qquad \text{for} \qquad C^{14}$$

$$(1p_{1/2})^2_{1^+} \qquad \text{for} \qquad N^{14}$$

By coupling a $d_{5/2}$ or $2s_{1/2}$ nucleon to $(1p_{1/2})^2_{J=0}$ (the C^{14} ground state) one obtains two A = 15 states, which are strongly populated in (d,n) on C^{14} with S = 1, whereas they are not seen in $N^{14}(d,n)O^{15}$, meaning S = 0.

By coupling the $d_{5/2}$ nucleon to $(1p_{1/2})^2_{J=1}$ (the ground state of N^{14}) one obtains three A = 15 states, and by coupling the $2s_{1/2}$ nucleon, two states. All five states, of cource, are strongly populated in $N^{14}(d,n)O^{15}$ with S = 1, while they are not expected to show up in $C^{14}(d,n)N^{15}$ reaction, meaning S = 0.

The shell model calculations of Halbert or Zuker et al. also predict two strong states in $C^{14}(d,n)N^{15}$ and five strong states in the $N^{14}(d,n)O^{15}$ reaction. Thus the mixed wave functions of the theory keep the qualitative features of pure jj-coupling in good agreement with experiment. The only exception is connected with the fifth state which should be seen but is not observed in the $N^{14}(d,n)O^{15}$ reaction. The question why experiment fails to observe the second strong $J^\pi = 3/2^+$ state in O^{15} remains open.

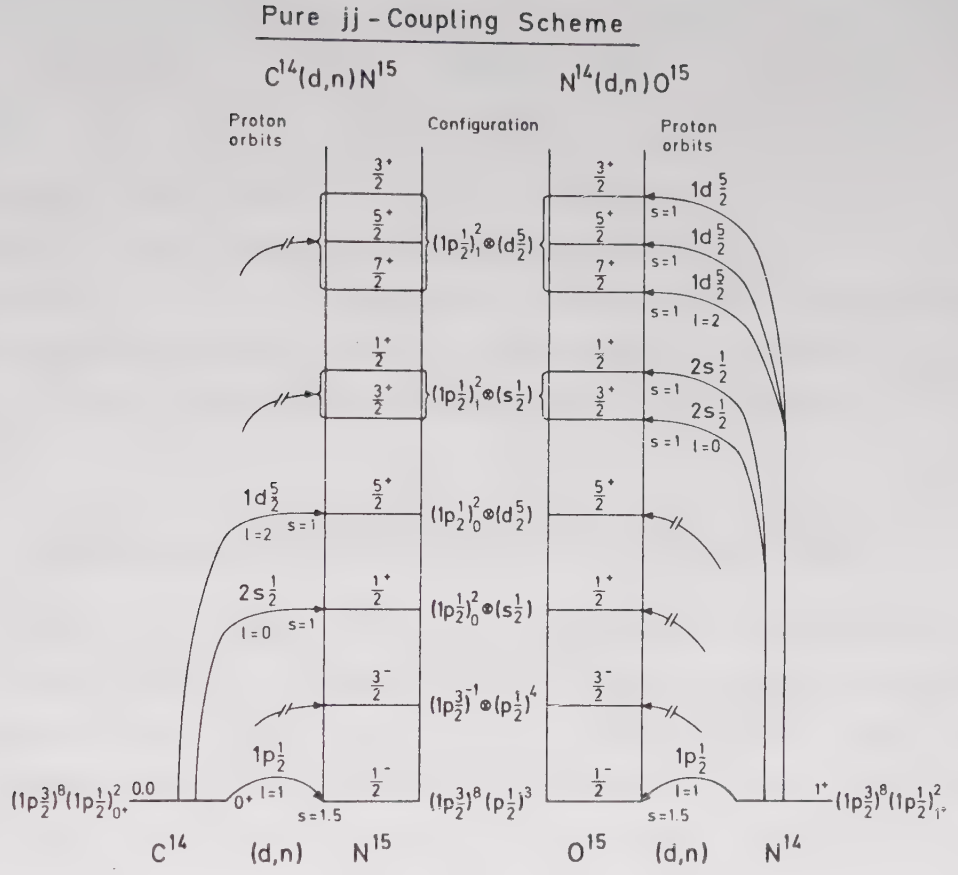

Fig.19 - Pure jj-coupling for the lowest states in the mirror nuclei N^{15} and O^{15} arising from $C^{14}(d,n)N^{15}$ and $N^{14}(d,n)O^{15}$ reactions. S - the expected spectroscopic factor of the state. Broken arrows indicate forbidden transitions.

The experimental spectroscopic factors for N^{15} show evidence of configuration mixing. This is qualitatively in agreement with the theoretical calculations, but quantitatively the mixing exceeds the prediction as can be seen in the S-values of the states not to be populated in pure jj-coupling. Especially that of the 6.324 MeV negative-parity state which is forbidden in pure jj-coupling shows the presence of a $(p_{3/2})^6 (p_{1/2})^4$ core excited component in the C^{14} ground state in qualitative agreement with the wave functions of Cohen and Kurath. Quantitatively the experimental spectroscopic factor of this state is a factor of 3 greater than that of Cohen and Kurath, which suggests the influence of some other process that might for instance be attributed to a (d,n) ground state transition with the outgoing neutron subsequently exciting a particle out of the $p_{3/2}$ into the $p_{1/2}$ level thus resulting in a two-step process.

6.2.2 S-factor Discrepancy and the Isospin Problem

Figuring in Table 6.1 is the following discrepancy: The S-factors for the lowest T = 0 states are approximately the same for the (d,n) and the (He^3,d) reaction on C^{13} while for the T = 1 states, the S-value from the (d,n) reaction is notably smaller than that from the (He^3,d) reaction, an anomaly observed also by Siemssen et al.(Si66) for light nuclei and recently reported by Kozub and Youngblood (Ko72) for molybdenum isotopes in a (p,d) and (d,t) reaction comparison.

In an attempt to account for this discrepancy, Tamura (Ta67) included charge exchange affects or the isospin-coupling potential $V(\vec{t}.\vec{T})$ in the DWBA optical potential (this has been here neglected), which can reduce the theoretical cross-section, and thus bring an increase of about a factor of 2 into the experimental S-factor. This is based on the existence of a distructive interference between the neutron groups arising from the two competing processes in the reaction e.g.

$$C^{13} + d \begin{cases} \nearrow\ N^{14} + n & \text{direct process,} \\ \searrow\ (C^{14} + p) \longrightarrow N^{14} + n & \text{exchange process,} \end{cases}$$

where the latter process is brought about by isospin-exchange. Since, however, the influence of this coupling goes in the same direction for $T_<$ and $T_>$ final states, it cannot account for the observed discrepancy.

With regard to this discrepancy, Cotanch and Robson (Co73) have recently attributed this anomaly, namely, $S(d,n) < S(He^3,d)$ for $T = 1$ transitions, to the difference in the imaginary absorption potential W for the (He^3,d) reaction leading to states of different isospin. The imaginary potential $W = i\Gamma^{\downarrow}/2$, is dependent on the spreading width $\Gamma^{\downarrow}$, which is proportional to the level density $\rho(E)$ of the compound system.

In the compound nucleus formed by A + a during the reaction A(a,b)B, the level density $\rho(E)$ is greater for $T_<$ states than for $T_>$ states at the same energy. Assuming isospin conservation, there are many more available $T_<$ channels than $T_>$ channels to absorb flux, where

$$T_< = T_A - t_a = T_B - t_b$$

$$T_> = T_A + t_a = T_B + t_b \qquad 6.2.1$$

Hence

$$\rho_{T_<}(E) > \rho_{T_>}(E) \rightarrow W(T_<) > W(T_>) \rightarrow \sigma(T_<) < \sigma(T_>) \qquad 6.2.2$$

For the (d,n) reaction, there is only one type of absorption effective, namely with $T = 1/2$ in the case of

$$C^{13}_{T=1/2} + d_{T=0} \begin{cases} \nearrow N^{14}_{T=0} + n_{T=1/2} \\ \searrow N^{14}_{T=1} + n_{T=1/2} \end{cases}$$

for both $T = 0$ and $T = 1$ final states. But for the (He^3,d) reaction there are two different types of absorption with $T = 0$ and $T = 1$ respectively as follows:

$$C^{13}_{T=1/2} + He^{3}_{T=1/2} \begin{cases} \rightarrow N^{14}_{T=0} + d_{T=0}\,, & T_< = 0 \text{ in the compound system,} \\ \rightarrow N^{14}_{T=1} + d_{T=0}\,, & T_> = 1 \text{ in the compound system.} \end{cases}$$

The effect of having a larger (smaller) absorption for $T_<$ ($T_>$) states in (He^3,d) reaction leads to a smaller (larger) theoretical cross-section than given by the simple DWBA and consequently will reduce or influence the S-factor for (He^3,d) reaction while that of (d,n) remains unaffected since only one T and therefore only one type of deuteron absorption is possible.

6.3 (d,n) Stripping to Unbound States and (p,p) Elastic Scattering

In a (d,p) reaction on N^{15}, Fuchs et al. (Fu72) observed a parallelism between (d,p) stripping and (n,n) elastic scattering, namely, between the proton spectra and energy dependence of the total neutron cross-section. The parallelism holds also for the shape of the interference between resonances and the continuum, thus confirming Lipperheide's theory (Li70) that in the reaction A(d,p)B the proton spectrum in PWBA is given by the total off-energy-shell neutron cross-section σ^{tot}_{nA}, expressed in the form

$$\frac{d\sigma_p(E_p)}{d\Omega dE_p} = \frac{1}{k^2}\,\sigma^{tot}_{nA}(q_n,E_n) \qquad \text{off-shell} \qquad 6.3.1$$

where

k = $q^2/(2m - E_p)$ - the neutron wave number,

$q(\theta)$ = momentum transfer,

E_n = $(E_d - E_p - 2.224)$ MeV, - energy of the neutron in the residual system B + n,

$E_n = \frac{\vec{p}^2}{2m}$ for "on-shell", and is valid for a free neutron with momentum $\vec{p}$

$E_n < \frac{\vec{p}^2}{2m}$ for "off-shell",

$S \equiv \frac{\vec{p}^2}{2m} - E_n$, "off-shell" variable.

For (n,n) elastic scattering, the on-shell total neutron cross-section (in case of target with zero spin) is given by

$$(\sigma_{nA}^{tot})_{on\text{-}shell} = \frac{4\pi}{k^2} \sum_{J^\pi} (2J + 1) \sin^2 \delta_\ell^{nucl} \qquad 6.3.2$$

where δ_ℓ^{nucl} - the nuclear scattering phase shift for the captured neutron,

J^π - the spin-parity of the partial waves.

The purpose of this work was also to search for a similar parallelism between the (d,n) stripping and the (p,p) elastic scattering in the relation

$$\frac{d\sigma(E_n)}{d\Omega dE_n} = \frac{1}{k^2} \sigma_{pA}^{tot}(q_p, E_p) \qquad \text{off-shell} \qquad 6.3.3$$

and

$$(\tilde{\sigma}_{pA}^{tot})_{on\text{-}shell} = \frac{4\pi}{k^2} \sum_{J^\pi} (2J + 1) \sin^2 \delta_\ell^{nucl} \qquad 6.3.4$$

where δ_ℓ^{nucl} - the nuclear scattering phase shift for proton.

Since for (p,p) scattering, the total cross-section is not measurable because of the diverging Coulomb scattering, an artificial proton total cross-section can, after correcting for the Coulomb phase shift, be defined for a particular partial wave ℓ as

$$(\tilde{\sigma}_{pA}^{tot})_\ell = \frac{4\pi}{k^2}(2J + 1) \sin^2 \delta_\ell^{nucl} \propto \frac{\sin^2 \delta_\ell^{nucl}}{E_p} \qquad 6.3.5$$

with $\delta_\ell = \delta_\ell^{nucl} + \delta_\ell^{Coul}$ as the total phase shift and

δ_ℓ^{Coul} - the Coulomb phase shift.

This is justifiable since such a relation is valid for neutrons. Taken the nuclear phase shift δ_ℓ^{nucl} from measurement,

$\frac{1}{k^2}\sin^2\delta_\ell^{nucl}$ can then be calculated. This is what has been done in this work for the $C^{12}(d,n)N^{13}$ transition to the $s_{1/2}$ resonance state with δ_ℓ^{nucl} taken from the measurement of Jackson et al. (Ja53) for the (p,p_o) elastic scattering.

Fig.20 (identical to Fig.5) shows the search for this similarity between (d,n) stripping and (p,p) elastic scattering. The s-resonance shape of the 2.366 MeV unbound state, has indeed the form of $\sin^2\delta_\ell^{nucl}$ calculated from the experimental δ_ℓ^{nucl} represented by the heavy solid line in Fig.20

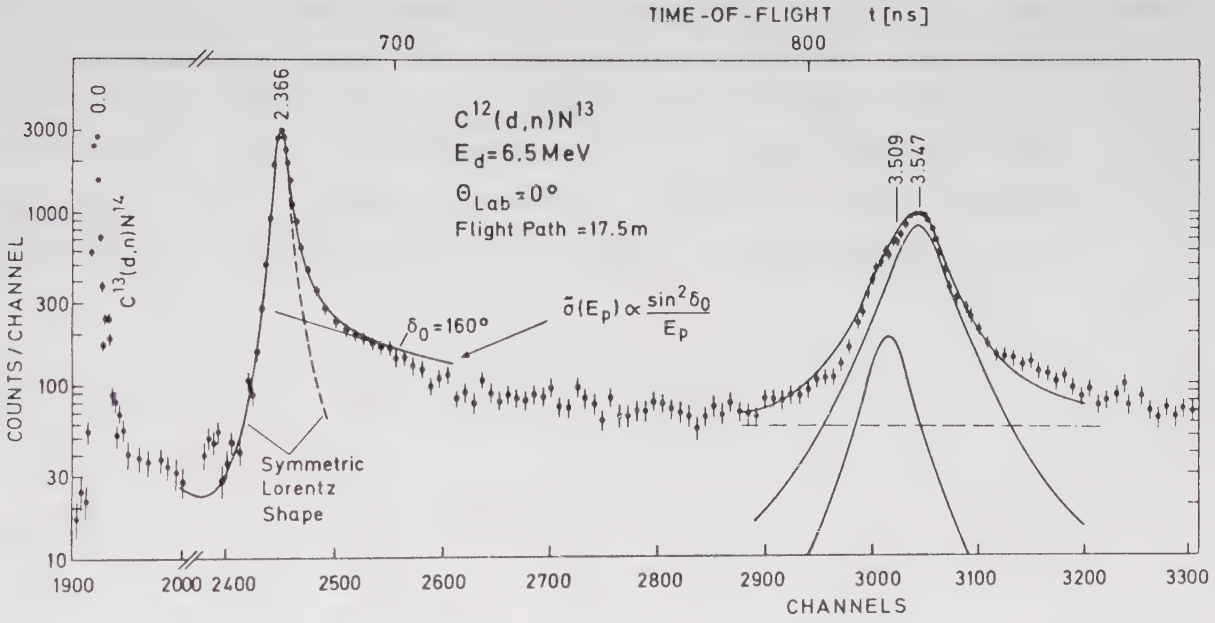

Fig.20 - Relationship between the $C^{12}(d,n)N^{13}$ stripping to the s-wave resonance at E_x = 2.366 MeV in N^{13} and the corresponding (p,p) elastic scattering. The cross-section calculated from the exponential (p,p) phase shift according to Eq.6.3.5 is shown as solid curve for this resonance.

The assymmetry is connected mainly with the nearly constant phase δ_o^{nucl} of 160° exhibited above resonance in the (p,p_o) elastic scattering measurement (Ja53). This offers the conclusion that there is a parallelism between (d,n) stripping to unbound states and the (p,p) elastic scattering similar to that between (d,p) and the (n,n), thus confirming the theory of Lipperheide for protons too. A similar strong and probably assymmetric s-wave structure was observed in the $C^{13}(d,n)N^{14}$ reaction at E_x = 8.061 MeV .

6.4 The (d,n) to (p,p) Cross-section Ratio

Fuchs et al. (Fu72) also discovered that the ratio of the (d,p) stripping cross-section to that of the (n,n) elastic scattering increases with the transition l-values. The question whether the (d,n) to (p,p) cross-section ratio behaves in the same way was also of interest in this work. Shown in Fig.21 for all three (d,n) reactions on the carbon isotopes leading to $C^{12,13,14}$ + p are the (d,n) to (p,p) cross-section ratio

$$F = \frac{d\sigma}{d\Omega}(d,n) \Big/ \frac{(2J_f + 1)\Gamma_p}{(2J_i + 1)E_p} \qquad 6.4.1$$

where
- Γ_p - the partial resonance width for proton emission taken from (p,p) scattering,
- E_p - the proton energy,
- J_i, J_f - the initial and final spin of the target and residual nucleus.

The artificial total proton cross-section of the l-th partial wave, $\frac{2J_f + 1}{2J_i + 1}\frac{\Gamma_p}{E_p}$, has been defined in analogy to the considerations of Sect.6.3. The denominator $(2J_i + 1)$ has been introduced because of the non-zero target spin of $C^{13}(J^\pi = 1/2^-)$.

AS seen in Fig.21 the F-values for the same l lie on a smooth curve, and increases with increasing l-value (except for one l = 2 state in C^{13} + p which is not understood).

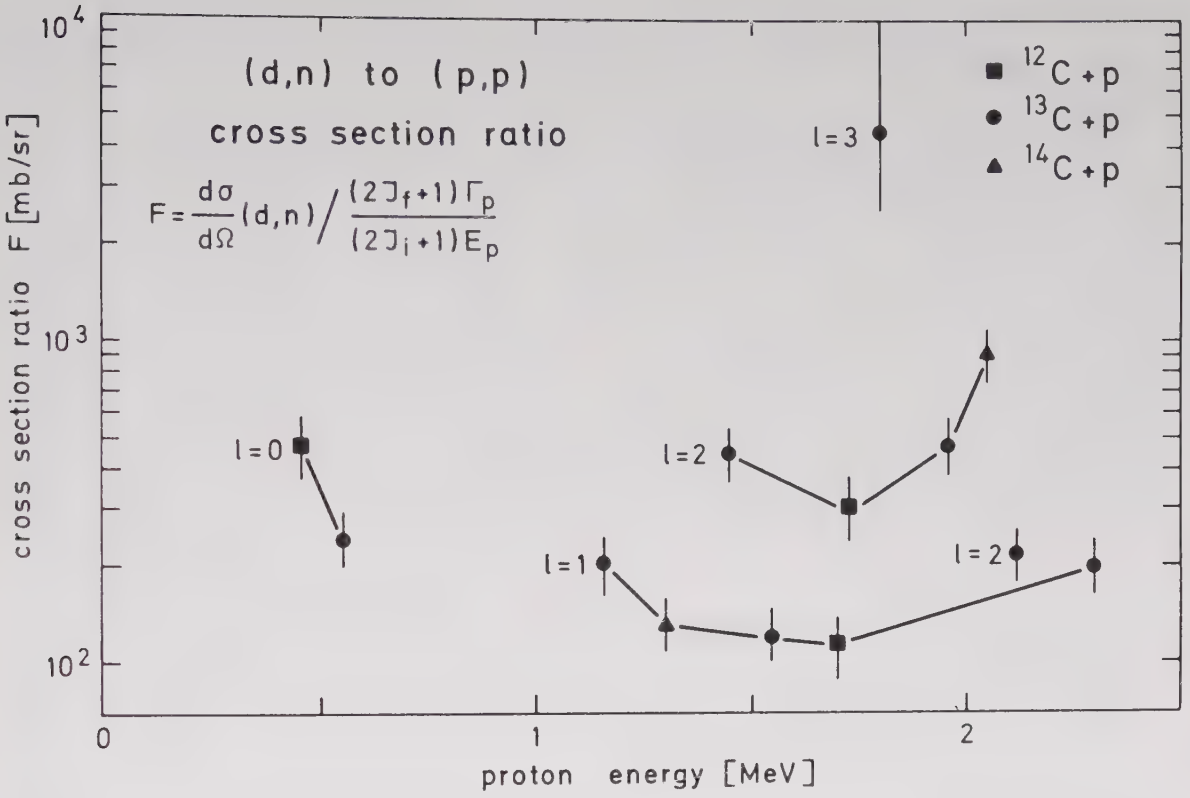

Fig.21 - (d,n) to (p,p) cross-section ratio dependence on the transferred resonance angular momentum l.

The interpretation of this increase with l-value is that in (d,n) stripping, the proton has more momentum for reaching a given resonance than in the (p,p) elastic scattering. Therefore in the (d,n), a state of higher l-value can be more easily formed. The (d,n) to (p,p) cross-section ratio thus offers a single handed fast method for l-value assignment for a collection of nuclei through (d,n) stripping on a collection of (preferably zero spin) targets which can be based on a single angle e.g. the zero-degree measurement.

CHAPTER 7

SUMMARY AND CONCLUSIONS

Through one-nucleon-transfer, this work has investigated the structure of the nitrogen isotopes $N^{13,14,15}$-bound and unbound states, with consequent spin and parity identification of the investigated states and extraction of spectroscopic factors. It has thus tested the validity of the DWBA and Hauser-Feshbach theories in describing direct and CN interactions and checked the extent to which the nucleus is described by the shell model wave functions in simple jj-coupling or with configuration mixing. It also studied the resonance stucture of the unbound systems $p + C^{12,13,14}$ as well as the relation between (d,n) and (p,p) elastic scattering with respect to the transferred resonance angular momentum.

The high bombarding deuteron energy of 6.5 MeV enabled levels up to E_x = 9.702 MeV excitation energy in N^{14} and E_x = 12.097 MeV in N^{15} to be reached, respectively, in the $C^{13}(d,n)N^{14}$ and $C^{14}(d,n)N^{15}$ reactions. With some states obscured by C^{12} and O^{16} contaminations, angular distributions were obtained for transitions to nineteen final states in N^{14} and twenty one states in N^{15} including a new state at 11.44 MeV excitation energy. For the first time, the states of N^{15}, apart from the lowest four, have been investigated through proton transfer on C^{14}.

The angular distributions have been analysed using the DWBA and Hauser-Feshbach calculations with the latter freely normalized. In the incident channel, the optical-potential parameters for the deuteron were systematically searched for until the best fit of theory with experiment was obtained while the exit channel neutron parameters were taken from Hodgson. With the DWBA analysis, the transferred angular momenta were determined and the resulting J^{π}-values discussed.

For the N^{14} the l-values obtained from the angular distributions are compatible with the already known spin and parity information and for the first time, spectroscopic factors for states above E_x = 8.907 MeV excitation energy have been obtained, and theoretical spin and parity assignments for these states confirmed through proton transfer on C^{13}.

In case of N^{15}, the DWBA analysis gave l-values compatible with the already known spins and parities of the previously investigated four states, and a series of new spins and parities as well as new spectroscopic factors. The 9.155 MeV and 9.225 MeV states have been identified to be of positive parity populated through $l_p = 2$ proton transfer and assigned with $J^\pi = 5/2^+$ and $J^\pi = (3/2, 5/2)^+$ respectively, while the high spin state of 8.829 MeV is favoured with positive parity and hence $J^\pi = 7/2^+$, resulting probably from an $l_p = 4$ proton transfer. The controversial 9.929 MeV state has appeared here convincingly $l_p = 0$ populated and thus assigned with $J^\pi = 1/2^+$, and the same for the 10.451 MeV state. The new state of 11.44 MeV has been assigned with $l_p = 2$, $J^\pi = 3/2^+$ or $l_p = 3$, $J^\pi = 5/2^-$, while states like the 10.536 MeV and 11.236 MeV remain ambiguous or still undecided.

The S-factor anomaly in the relation between (d,n) and (He^3,d) stripping to the T = 1 states in N^{14} has been observed, and the discrepancy attributed to isospin coupling influence giving rise to differences in the absorption potential.

The comparison of S-factors for N^{15} with those of its mirror nucleus O^{15} and theory based on simple jj-coupling scheme has revealed significant correlations between the transition strengths of the analog states in these mirror nuclei, and pinpointed a prominent discrepancy in the failure of experiment to observe the theoretically strongly populated $J^\pi = 3/2^+$ state in O^{15}. With the use of the simple jj-coupling, an insight has been given into the dominant configuration of the lowest states with positive parity (π = +) in A = 15 nuclei

which consists of a $2s_{1/2}$ or $1d_{5/2}$ nucleon coupled to the A = 14 system in the $(1p_{1/2})^2_{J^\pi=0^+,1^+}$ ground states. Contrary to the pure jj-coupling, the extracted experimental S-factors show evidence of configuration mixing.

In stripping to unbound states, the resonance structure of the systems $C^{12,13,14}$ + p in the (d,n) reaction, studied in comparison with corresponding resonances from (p,p) elastic scattering in order to establish a relation between the (d,n) and (p,p) similar to the parallelism between the (d,p) and (n,n) observed by Fuchs et al., has confirmed that Lipperheide's theory is also valid for the relation between (d,n) and (p,p) and actually, the unbound states neutron spectrum and cross-section are qualitatively given by the total off-energy shell proton cross-section.

The (d,n) to (p,p) cross-section ratio also evaluated for all three reactions $C^{12,13,14}$(d,n)$N^{13,14,15}$ revealed a dependence on l-values and increases with the transferred resonance angular momentum leading to the conclusion that the transferred proton in the (d,n) stripping is endowed with higher momentum than in the (p,p) elastic scattering thus enhancing the easy formation of a state of higher l-value . The (d,n) to (p,p) cross-section ratio has been confirmed to offer a quick method for l-value assignment for states in a collection of nuclei through (d,n) stripping on a collection of targets with measurements sufficient at one angle only.

On the whole, the results of this work have extended the existing knowledge on the structure of the nitrogen isotopes $N^{13,14,15}$-bound and unbound states. Moreover, interest could be excited in some more work to check the spin and parity of those states in N^{15} still remaining ambiguous after this work, and the failure of experiment to observe the theoretically strong $J^\pi = 3/2^+$ state in O^{15}.

REFERENCES

Aj 70 - Ajzenbrg-Selove F., Nucl. Phys. A152 (1970) 97

Al 69 - Alford W.P., and Purser K.H., Nucl. Phys. A132 (1969) 86

Au 55 - Auerbach T., and French J.B., Phys. Rev. 98 (1955) 1276

AU 62 - Austern N., in Fast Neutron Physics II
(Interscience Publishers, New York 1962)

Ba 62 - Bassel R.H., et al., The Distorted-Wave Theory of
Direct Nuclear Reactions. Oak Ridge National Lab.
(Oak Ridge, Tennessee 1962)

Bi 52 - Biedenharn L.C., Blatt J.M., and Rose M.E.,
Rev. Mod. Phys. 24 (1952) 249

Bi 53 - Biedenharn L.C., and Rose M.E., Phys. Rev. 25 (1953) 729

Bo 71 - Bommer J., Fuchs H., Grabisch K., Janetzki U., and
Röschert G., Nucl. Phys. A172 (1971) 618

Bo 73 - Bobbitt J.R., Etten M.P., and Lenz G.H.,
Nucl. Phys. A203 (1973) 353

Br 69 - Brown G.I., Comments on Nuclear and Particle Physics 3
(1969) 136

Bu 73 - Busse et al., Jahresbericht 1972, HMI-P, Berlin

Co 56 - Condon & Shortly, The Theory of Atomic Spectra

Co 67 - Cohen S., and Kurath D., Nucl. Phys. A101 (1967) 1
73 (1965) 1

Co 68 - Cookson J.A., Phys. Lett. 27B (1968) 619

Co 69 - Cords H., Din G.U., and Robson B.A.,
Nucl. Phys. A127(1969)95, A134(1969)561

De 57 - Devons S., and Goldhaber L.J.B., "Angular Correlations"
in Handbuch der Physik Vol. 42, P.362ff.
Ed. Fleige S., (Springer, Berlin 1957)

Fe 60 - Feshbach H., "The Compound Nucleus" in Nuclear
Spectroscopy Part B. P.625, Ed. Ajzenberg-Selove F.,
(Academic Press, New York and London 1960)

Fe 65 - Feshbach H., Direct Interaction and Nuclear Structure
Mechanisms. P.251. Ed. Clemental E., and Villi C.,
Padua 1962

Fo 71 - Fortune H.T., Middleton R., Garrett J.D., and
Halbrow C.H., Phys. Rev. C3 (1971) 1441

Fr 65 - French J.B., Phys. Rev. 103 (1956) 1391

Fr 61 - French J.B., Macfarlane M.H., Nucl. Phys. 26 (1961) 168

Fu 66 - Fuchs H., Grabisch K., Kraaz P., and Röschert G., Phys. Lett. 23 (1966) 363

Fu 67 - Fuchs H., and Sonto R., Phys. Lett 24 B (1967) 234

Fu 72 - Fuchs H, Homeyer H., Oschler H., Lipperheide R., and Möhring K., Nucl. Phys. A 196 (1972) 286

Gr 72 - Grabisch K., Doktorarbeit, HMI-P, Berlin 1972

Ha 52 - Hauser W., and Feshbach H., Phys. Rev. 87 (1952) 366

Ha 57 - Halbert E.C., and French J.B., Phys. Rev. 105 (1957) 1563 and Ph. D. Thesis, Oak Ridge National Laboratory Oak Ridge, Tennessee

Ha 66 - Haag D. Laborbericht Nr. 4, HMI-P Berlin 1966

Ho 66 - Holbrow C.H., Middleton R., and Rosner R., Phys. Rev. 152 (1966) 970

Ho 69 - Holbrow C.H., Middleton R., and Focht W., Phys. Rev. 183 (1969) 880

Ho 71 - Hodgson P.E., Nuclear Reactions and Nuclear Structure. P 179 (Clarendon Press Oxford 1971)

Hu 59 - Hull M., and Breit G., Encyclopedia of Physics Vol 41, Ed. Flüge S., (Springer Verlag Berlin 1959)

Hu 65 - Huby R., and Mines J.R., Rev. Mod. Phys. 37 (1965) 406

Ja 53 - Jackson H.L., and Galonski A.I., Phys. Rev. 89 (1953) 370

Ja 54 - Jancovici B., and Talni I., Phys. Rev. 95 (1954) 289

Kl 71 - Kluge H., Diplomarbeit, HMI-P, Berlin 1971

Kl 72 - Kluge H., Laborbericht, HMI-P, Berlin 1972

Ko 72 - Kozub R.L. and Youngblood D.H, Phys. Rev.Lett.28(1972)1529

Ku 67 - Kunz P.D., DWBA-Code: DWUCK, University of Colorado 1967, unpublished , amended by Nucl. Research Centre, University of Alberta 1967 and by G. Röschert, Hahn-Meitner-Institut Berlin 1970

La 67 - Lavergren B., and Mitchel I.V., Nucl. Phys. A 98 (1967) 481

Li 70 - Lipperheide R., Phys. Lett. 32 B (1970) 555

Li 71 - Lie S., and Engeland T., Nucl. Phys. A 169(1971)617

Ma 68 - Marion J.B., and Young F.C., Nucl. Reactions Analysis P. 154, 211. (North Holland Publ. Company Amsterdam 1968)

Ma 69 - Marmier P., and Sheldon E., Physics of the Nuclei and Particles Vol. 1 (1969) 485 (Academic Press, New York)

Ma 73 - Mairle G., and Wagner G.J., Z. Phys. 258(1973)321

Mc 70 - Mckellar B.H.J., Phys. Lett. 32B(1970)246

Mo 63 - Mobley R.C., Rev. Sci. Lustr. 34 (1963), 256

Mu 67 - Mubarakmand S., and Maccfield B.E.F., Nucl. Phys. A 98 (1967) 82

Mu 71 - Mutchler G.S., Rendie D., Velkley D.E., Sweeney Fr.W.E., and Phillips G.C., Nucl. Phys. A 172 (1971) 469

NIM 72 - Nucl. Instr. Meth. 101 (1972) 519

Pe 62 - Perey F., and Buck, Nucl. Phys. 32 (1962) 353

Pi 72 - Pietrzyk P., Laborbericht 13 (1972) 1 HMI-P Berlin

Pr 64 - Price W.R., Nucl. Radiation Detection. P 127 (McGraw Hill Book Company New York 1964)

Rö 65 - Röschert G., Diplomarbeit 1965, HMI-P, Berlin

Rö 70 - Röschert G., Laborbericht 12 (1970) 1, HMI-P Berlin

Sa 56 - Satchler G.R., Phys. Rev. 104 (1956) 1198 erratum Phys. Rev. 111 (1958) 1474

Sa 64 - Satchler G.R., Nucl. Phys. 55 (1964) 1

Sa 65 - Satchler G.R., Lecture Notes for the 1965 Summer Institute for Theoretical Physics. University of Colorado, Boulder, Colorado

Sc 60 - Schwarz C.D., and Oven G.E., in Fast Neutron Phys. Part 1 (1960) 211 (Interscience Publishers, N. York (1960)

Se 63 - Sebe T., Prog. Theor. Phys. Tap. 30 (1963) 290

Sh 55 - Sherr R., Gerhart J.B., Horie H., and Hornyab W.F., Phys. Rev. 100 (1955) 945

Si 66 - Siemssen R.H., Morrison G.C., Ziedman B., and Fuchs H., Phys. Rev. Lett. 16 (1966) 1050

Si 72 - Sichelschmidt, Vorläufige Programmbeschreibung für OPTIMA, HMI-P, Berlin 1972, unpublished

Ta 60 - Talmi I., and Una I., Ann. Rev. Nucl. Sci. 10 (1960) 353

Ta 67 - Tamura T., Phys. Rev. Lett. 19 (1967) 321
Phys. Rev. 165 (1968) 1123

Te 66 - Tepel J.W., Nucl. Instr. Method 40 (1966) 100

To 59 - Tobocman W., Phys. Rev. 115 (1959) 98

To 61 - Tobocman W., Theory of Direct Nuclear Reactions
(Oxford University Press 1961)

Tr 63 - True W.W., Phys. Rev. 130 (1963) 1530

Vi 70 - Vincent C. M., and Fortune H.T., Phys. Rev. C2 (1970) 782

Vo 68 - Vogt E., " The statistical Theory of Nuclear Reactions"
in Advances in Nuclear Physics Vol.1 P. 261
Ed. Baranger M., and Vogt E., (Plenum Press, New York)

Wa 60 - Warburton E.K., and Pinkston W.T.,
Phys. Rev. 118 (1960) 733

Zu 69 - Zuker A.P., Buck B., and McGrory J.B., " Shell Model
Wavefunctions for A = 15-18 Nuclei". Informal Report
PD-99 BNL 1485(1969)1, (Brookhave National Lab.,
Upton, New York, Oak Ridge National Lab., Oak Ridge,
Tennessee)

AKNOWLEDGEMENTS

May I thank Prof. E. Finckh for offering me the opportunity to come into Hahn-Meitner Institute, and Dr. H. Fuchs for his strong encouragements and marvellous assistance that led me to accomplish this work, and above all, Prof. K. H. Lindenberger for his constant support of this work and for the condusive conditions made available to me for this work in Hahn-Meitner Institute.

My thanks also to all others whose contributions enhanced the accomplishment of this work, specially to Mr. E. W. Rebmann for reproducing the finished copies, to Hahn-Meitner Institute and the Free University of Berlin for financial support, and to all German people for the experiences I accumulated here.

AUTOBIOGRAPHY

In 1940, July 5, I was born to the family of Chief Michael Ekpo and his wife, Madame Finhas Ekpo (from the house of Udo Ette), in Ikot Essen Akpantuen, South Eastern State, Nigeria.

In 1946, I started my primary education in Ikono No.1 School in Ikot Essen Akpantuen, where I obtained my "First School Leaving Certificate" in 1953.

In 1954, Jan., I went to the Lutheran High School in Obot Idim, Uyo, where I finished my high school education in 1959 with the "West African School Certificate" obtained from the University of Cambridge, England.

The years 1960 to 1963 offered me including some technical training in West Germany, my first after-school experiences as a laboratory technologist in the Laboratory Department of the Ministry of Commerce and Industries, Enugu, Nigeria.

1964 saw the beginning of my studies in the University of Warsaw, Poland, where in 1969, I obtained my Master of Science, M.Sc., Degree in Nuclear Physics.

1969, June, witnessed my marriage to Jolanta Stachowicz from Warsaw, Poland.

In 1969, Nov., I was employed as a research scientist in Hahn-Meitner Institute, West Berlin, and under the auspicies of Prof. Lindenberger, I was offered a research opportunity in Nuclear Physics for the Doctorate Degree from the Free University, Berlin.